Cerebral Cortex July 2015;25:1842–1857
doi:10.1093/cercor/bht426
Advance Access publication January 22, 2014

miRNAs are Essential for the Survival and Maturation of Cortical Interneurons

Sebnem N. Tuncdemir[1], Gord Fishell[1] and Renata Batista-Brito[1,2]

[1]NYU Neuroscience Institute and the Department of Neuroscience and Physiology, Smilow Research Center, New York University School of Medicine, New York, NY 10016, USA and [2]Current Address: Department of Neurobiology, Yale University, PO Box 208001, New Haven, CT 06520-8001, USA

Address correspondence to Dr Gord Fishell or Dr Renata Batista-Brito, NYU Neuroscience Institute and the Department of Neuroscience and Physiology, Smilow Research Center, New York University School of Medicine, 522 First Avenue, New York, NY 10016, USA. Email: fisheg01@nyumc.org, gordon.fishell@med.nyu.edu or renata.brito@yale.edu

Complex and precisely orchestrated genetic programs contribute to the generation, migration, and maturation of cortical GABAergic interneurons (cIN). Yet, little is known about the signals that mediate the rapid alterations in gene expression that are required for cINs to transit through a series of developmental steps leading to their mature properties in the cortex. Here, we investigated the function of post-transcriptional regulation of gene expression by microRNAs on the development of cIN precursors. We find that conditional removal of the RNAseIII enzyme Dicer reduces the number of cINs in the adult mouse. Dicer is further necessary for the morphological and molecular maturation of cINs. Loss of mature miRNAs affects cINs development by impairing migration and differentiation of this cell type, while leaving proliferation of progenitors unperturbed. These developmental defects closely matched the abnormal expression of molecules involved in apoptosis and neuronal specification. In addition, we identified several miRNAs that are selectively upregulated in the postmitotic cINs, consistent with a role of miRNAs in the post-transcriptional control of the differentiation and apoptotic programs essential for cIN maturation. Thus, our results indicate that cIN progenitors require Dicer-dependent mechanisms to fine-tune the migration and maturation of cINs.

Keywords: cortical interneurons, dicer, microRNA, post-transcriptional regulation

Introduction

The complex functions of the cerebral cortex rely on neuronal networks of highly interconnected glutamatergic principal neurons and gamma-aminobutyric acid (GABAergic) interneurons (cIN). Although GABAergic cINs comprise a minority of neocortical neurons (~10–20% in rodents), they are essential for cortical function (Whittington and Traub 2003; Markram et al. 2004; Moore et al. 2010; Rudy et al. 2011) and have been associated with various neurological disorders (Levitt et al. 2004). Cortical INs display a remarkable diversity and can be classified based on their morphological, physiological, molecular, and synaptic features (Markram et al. 2004; Petilla Interneuron Nomenclature et al. 2008). Fast-spiking interneurons that express the calcium-binding protein parvalbumin (PV) and low threshold-spiking interneurons that express somatostatin (SST) are the 2 most abundant interneuron subtypes in the cortex (Rudy et al. 2011), and originate in the medial ganglionic eminence (MGE) of the subpallium (Nery et al. 2002; Polleux et al. 2002; Ang et al. 2003; Butt et al. 2008; Batista-Brito and Fishell 2009). To reach the cortex, cINs undergo a well-orchestrated set of events that likely require dynamic mechanisms to finely regulate the proper expression of specific genetic programs to facilitate these transitions. However, the molecular mechanisms involved in coordination of events mediating cIN development such as migration and differentiation are not well understood.

MicroRNAs (miRNAs) are a class of small noncoding RNAs that act as post-transcriptional regulators of gene expression. miRNAs function by reducing translational efficiency or directing the targeted degradation of mRNAs (Filipowicz et al. 2008). In mammals, the production of most miRNAs is dependent on the enzymes Drosha and Dicer. A single miRNA can downregulate multiple target genes simultaneously and thus can individually function as global regulators of gene expression (Krek et al. 2005; Lewis et al. 2005). The nervous system expresses a large number of miRNAs, some of which have been shown to play roles during neurogenesis, specification of neuronal fate, morphogenesis, synaptogenesis, and neurodegeneration (Krichevsky et al. 2003; Miska et al. 2004; Gao 2008; Fineberg et al. 2009; de Chevigny et al. 2012; Volvert et al. 2012). Removal of the Dicer enzyme or even a single miRNA (miR-9) (Shibata et al. 2008) within the pallium results in reduced cortical proliferation and thickness, as well as defective layering (De Pietri Tonelli et al. 2008), as well as abnormal Cajal–Retzius cell differentiation (Shibata et al. 2008). Moreover, postmitotic depletion of Dicer in excitatory forebrain neurons results in microcephaly and abnormal neuronal morphology (Davis et al. 2008).

Despite the relatively well-known roles of miRNAs in cortical excitatory cell development, the requirement of miRNAs in GABAergic cIN development have not been explored. To this end, we ablated *Dicer* either within the MGE progenitor domain or in postmitotic MGE-derived cINs. Our results demonstrated that inactivation of Dicer in MGE-derived cINs does not affect their proliferation; however, it causes progressive and widespread abnormalities in cIN survival, migration, and specification.

Materials and Methods

Mouse Strains

All animal handling and maintenance were performed according to the regulations of the Institutional Animal Care and Use Committee of the NYU School of Medicine. The $Nkx2.1^{Cre}$, $Lhx6^{Cre}$, $Dicer^{C/+}$, $RCE^{EGFP/+}$, transgenic lines were maintained on a mixed background (Swiss Webster and C57/B16). Genotyping was performed as previously described (Harfe et al. 2005; Fogarty et al. 2007; Xu et al. 2008; Sousa et al. 2009). $Dicer^{-/+}$; $Nkx2.1^{Cre}$ or $Dicer^{-/+}$; $Lhx6^{Cre}$ mice were crossed to $Dicer^{C/C}$; $RCE^{EGFP/EGFP}$ mice to generate $Dicer^{C/+}$; $Nkx2.1^{Cre}$; $RCE^{EGFP/+}$ (control) and $Dicer^{C/-}$; $Nkx2.1^{Cre}$; $RCE^{EGFP/+}$ (mutant); or $Dicer^{C/+}$; $Lhx6^{Cre}$; $RCE^{EGFP/+}$ (control) and $Dicer^{C/-}$; $Lhx6^{Cre}$; $RCE^{EGFP/+}$ (mutant) offspring.

Immunohistochemistry

Dicer mutant embryonic (E13.5, E15.5, E18.5) and postnatal animals (P18–21) were examined using immunohistochemistry ($n = 3$–5).

Brains were fixed by transcardiac perfusion with 4% paraformaldehyde (PFA)/phosphate-buffered saline (PBS) solution followed by a 1-h postfixation on ice with 4% PFA/PBS solution. Brains were rinsed with PBS and cryoprotected by using 30% sucrose/PBS solution overnight at 4 °C. Tissues were embedded in Tissue Tek, frozen on dry ice, and cryosectioned at 12 μm (for embryos) or 20 μm (for P18–P20) thickness. Sections for immunohistochemistry analysis were processed using 1.5% normal goat serum (NGS) and 0.1% Triton X-100 in all procedures except washing steps, where only PBS was used. Sections were blocked for 1 h, followed by incubation with the primary antibodies overnight at 4 °C. Cryostat tissue sections were stained with the following primary antibodies: Rabbit anti-enhanced green fluorescent protein (EGFP) (1:1000; Molecular Probes), rat anti-EGFP (1:1000, Nacalai Tesque), mouse anti-PV (1:1000; Sigma), rat anti-SST (1:250; Chemicon), rabbit anti-Vasoactive intestinal polypeptide (1:250; Incstar), mouse anti-Calretinin (1:1000; Chemicon), mouse anti-Reelin (CR50) (1:500; MBL), rabbit anti-cleaved Caspase3 (1:500; Cell Signaling), mouse anti-pH3 (1:500; Cell Signaling), rabbit anti-Tbr1 (1:500; abcam), rat anti-Ctip2 (1:1000; abcam), and rabbit anti-GABA (1:500, Sigma). Secondary antibodies conjugated with Alexa fluorescent dyes 488, 594 (Molecular Probes) raised from the same host used for blocking serum were applied for 1 h at room temperature for visualizing the signals. Nuclear counterstaining was performed with 100 ng/mL 4,6-diamidino-2-phenylindole (DAPI) solution in PBS for 5 min. Fluorescent images were captured using a cooled-CCD camera (Princeton Scientific Instruments, NJ, USA) using Metamorph software (Universal Imaging, Downingtown, PA, USA).

BrdU Histochemical Analysis for Cell Proliferation

Timed-pregnant females at E13.5 or E15.5 were given a single BrdU injection (1 mg BrdU/10 g mother) 1 h prior to sacrifice and removal of EGFP-positive embryos. Changes in cell proliferation within the MGE proliferative domain were assessed by performing double immunofluorescent labeling of BrdU and EGFP as follows: 12-μm cryosections were blocked using 10% NGS and 0.1% Triton X-100 in PBS for 1 h, and washed in PBS followed by incubation with rabbit anti-EGFP (1:500; Molecular Probes) in 1% NGS and 0.1% Triton X-100 in PBS overnight at 4 °C. Secondary antibody raised in goat anti-rabbit Alexa 488 (1:500; Molecular Probes) was applied for 1 h at room temperature (RT), followed immediately by postfixation in 4% PFA for 15 min at RT, HCl (0.5 N) for 6 min at 55 °C, fixation in 4% PFA for 10 min at RT, proteinase K (0.5 μg/mL) treatment for 4 min at 37 °C, fixation in 4% PFA for 15 min, with PBS washed in between each treatment. Sections were then blocked using 10% NGS and 0.1% Triton X-100 in PBS for 1 h, and washed in PBS followed by incubation with mouse anti-BrdU (1:100; BD Biosciences) in 1% NGS and 0.1% Triton X-100 in PBS overnight at 4 °C. Secondary antibody raised in goat anti-mouse Alexa 594 (1:500; Molecular Probes) was applied for 1 h at RT for visualizing the signals. Fluorescent images were captured using a cooled-CCD camera (Princeton Scientific Instruments) using Metamorph software (Universal Imaging).

In Situ Hybridization

All in situ hybridizations (ISHs) were performed as previously described (Hanashima et al. 2004) with the exception of miRNA-9 ISH (Volvert et al. 2012). For detection of miRNA-9, a DIG-labeled locked nucleic acid miRCURY hsa-miR-9 detection probe for the mature form of miRNA-9 was purchased from Exiqon (Vedbaek, Denmark), and the protocol was modified for embryonic tissue. The cDNA probes for *Gad67*, *Lhx6*, *Sst*, and *Npy* were available in the Fishell laboratory; cDNA for *Ebf1* was a kind gift of Dr Sonia Garel, which was subsequently linearized and RNA polymerase transcription was performed to obtain DIG-labeled antisense probes. Antisense probes for *Igf1* and *Gad65* were generated by PCR using specific primers with the 3′ primer containing T7 polymerase binding sequence: *igf1* (5′ primer: CTTGAGCAACCTGCAAAACA; 3′ primer: TGCTCTTAAGGAGGCC AAA), *Gad65* (TCTTTTCTCCTGGTGGCG; 3′ primer: TTGAGAGGCGG CTCATTC). Images were obtained by bright-field photography on a Zeiss Axioskop using Spot Advanced software. *Lhx6* and *Gad67* ISH signals were counted as described previously (Batista-Brito et al. 2009).

Data Collection and Statistical Analysis

All postnatal analysis was evaluated in the somatosensory barrel cortex. To minimize counting bias, we compared sections of equivalent bregma positions, defined according to the Paxinos and Franklin's Mouse Brain atlas. The total number of cells expressing Gad67, EGFP, and Lhx6 were counted for a defined optical area. Cortical layers were identified according to the density of DAPI nuclear staining. The percentages of cINs expressing subtype-specific markers among fate-mapped cells were calculated as a ratio between the number of double-positive cells (Marker and EGFP) over the total number of EGFP-positive cells. The areal density of cycling progenitors and cells in S phase, postmitotic cells in M phase, and caspase-3-positive apoptotic cells in the MGE of E13.5 and E15.5 of control and mutant mice were determined by counting $BrdU^+$, $PH3^+$, and $caspase3^+$ nuclear profiles, respectively, in a 100 × 100-μm box that was placed over the ventral MGE in region-matched mutant and control sections from 3 pairs of littermate embryos. Quantification of EGFP-positive cells in the cortex of E13.5, E15.5, and E18.5 brains were performed on 12-μm region-matched coronal ($n = 3–5$) sections of equivalent regions representing the embryonic somatosensory-motor regions according to the Jacobowitz and Abbott's atlas of the developing mouse brain. Embryonic layers, mantle zone (MZ), cortical plate (CP), and intermediate/subventricular zone (IZ/SVZ), were determined according to DAPI and Tbr1 staining. All data were represented as mean ± SEM, unpaired Student's *t*-test.

Cortex Dissection and Fluorescent-Activated Cell Sorting

Embryos obtained from timed-pregnant females were selected for dissection based on obtaining EGFP-positive signal within the subpallial region of the brains. Tissue samples were also collected for the identification of *Dicer* conditionally null mice. The cortices of E13.5 and E15.5 embryos were dissected in cold Dulbecco's modified eagle's medium (DMEM) and treated with 0.25% typsin (Wortington, Lakewood, NJ, USA) and DNaseI (0.1% Sigma, St. Luis, MO, USA) at 37 °C for 30 min. Dissociated cells from each embryo were then subjected to fluorescent-activated cell sorting (FACS) sorted based on the brightness of the EGFP signal (MoFlo, Beckman Coulter). For each sorting, we collected EGFP-positive ($EGFP^+$) and EGFP-negative ($EGFP^-$) cells, which were subsequently grouped based on the genotype and age of the animal. On average, the percentages of $EGFP^+$ cells were 2–4% for E13.5 cortex dissections, 6–8% for E15.5 cortex dissections, and 60–70% for E13.5 MGE dissections. In order to check for contamination in $EGFP^+$ and $EGFP^-$ sorted cells, we analyzed small samples of collected $EGFP^+$ and $EGFP^-$ populations under the microscope, which indicated that 95% purity was achieved in all cases. Collected cells were subsequently used for 1) examination of Dicer mRNA levels by RT-PCR, 2) quantification of miRNA levels by RT-PCR, 3) microarray analysis for miRNA expression levels, and 4) microarray analysis for mRNA expression levels.

RNA Preparation and Quantitative Real-time PCR for mRNA and miRNA Expression

For qRT-PCR to analyze *Dicer* gene expression, total RNAs from FACS-purified EGFP-positive cells were isolated using the QIAGEN RNeasy Mini Kit, then 100 μg total RNA was reversed transcribed using SuperScriptII First-strand Synthesis System (Invitrogen, Eugene, OR, USA). Equivalent volumes from RT samples were then used for SYBR Green incorporation qRT-PCR to detect mouse mRNA expression using the Power SYBR Green PCR system (Applied Biosystems) following manufacturer's instructions, normalized to *GAPDH* mRNA levels. Primers for *Dicer* are located in the exon deleted by Cre recombinase (Forward primer: ACCAGCGCTTAGAATTCCTGGGAG; Reverse primer: GCTCAGAGTCCATTCCTTGC) (Dugas et al. 2010), mouse GAPDH (Forward primer: TGTGTCCGTCGTGGATCTGA; Reverse primer: CCTGCTTCACCACCTTCTTGA). Quantitative assessment of the SYBR Green incorporation was done in Stratagene Mx3005*P*. Data was analyzed using the ddCt method (Livak and Schmittgen 2001). For qRT-PCR to analyze mature miRNA expression, total RNAs enriched in small RNA contents was isolated from FACS-purified EGFP-positive cells using the QIAGEN miRNeasy Mini Kit, then Taqman miRNA qRT-PCR analysis were performed on 10 ng of RNA for indicated miRNAs, using

miRNA-specific primers according to the manufacturer's protocol (Applied Biosystems) and normalized to the U6 snRNA. Quantitative assessment of the MGB probe incorporation was done in Stratagene Mx3005*P*. Data were analyzed using the ddCt method.

mRNA Microarray Expression Analysis

Total RNAs from FAC-sorted EGFP-positive cells from cortices of E15.5 *Dicer*$^{C/-}$; *Nkx2.1*^{Cre}; *RCE*^{EGFP} mutant embryos and 15.5 *Dicer*$^{C/+}$; *Nkx2.1*^{Cre}; *RCE*^{EGFP} controls were prepared by the TRIzol method (Invitrogen). Total extracted RNA (100 ng) was amplified and biotinylated using MessageAmp II-Biotin Kit (Ambion, Austin, TX), and hybridized to Affymetrix microarrays MOE430v2 (Affymetrix, Santa Clara, CA) containing 45 101 probe sets, carried out in the Genomics Core Lab at Memorial Sloan-Kettering Cancer Center (New York, NY, USA). Three independent datasets per RNA sample were produced for each genotype. Data processing of microarray expression analysis was performed as described previously (Cammenga et al. 2003; Rajasekhar et al. 2003; Batista-Brito et al. 2008) using the GeneSpring GX 10 software (Agilent, USA). To quantify the fold change (FC) of mRNA expression in mutants relative to controls, *Dicer*$^{C/-}$; *Nkx2.1*^{Cre}; *RCE*^{EGFP} and *Dicer*$^{C/+}$; *Nkx2.1*^{Cre}; *RCE*^{EGFP} microarrays were compared with each other. A two-tailed Student's *t*-test was then used for the calculation of the *P* value for each probe. We selected the genes that have a >2-fold decrease or increase with a $P < 0.01$. The results of this analysis are presented in Supplementary Table 2, as a direct comparison of raw average values from the above-mentioned control and mutant MGE-derived cells ($n = 3$ each).

miRNA Microarray Expression Analysis

The miRNA from FAC-sorted EGFP$^+$ and EGFP$^-$ cells from E13.5 MGE and E15.5 cortex was isolated, and 200 ng of miRNA was subsequently labeled, and hybridized to Agilent miRNA microarrays (Release 12.0), content sourced from Sanger miRBase (release 12.0), containing 627 mouse miRNAS and 39 mouse viral miRNAs. This procedure was repeated in triplicates to produce 3 independent datasets per miRNA sample. The microarray hybridization, data visualization and analysis were performed by the Genomics Core facility, MSKCC (New York, NY, USA). GeneSpring GX 10 software (Agilent) was used for value extraction. To assess if miRNA probes were differentially expressed in a pairwise comparsion of selected cell populations, a 2-fold enrichment cutoff and unpaired two-tailed Student's *t*-test was used to compare mean intensities between migratory MGE-derived cINs (E15.5 EGFP$^+$) and proliferating MGE-cINs (E13.5 EGFP$^+$); migratory MGE-derived cINs (E15.5 EGFP$^+$), and cortical non-MGE-derived cells (E15.5 EGFP$^-$); as well as proliferating MGE-cINs (E13.5 EGFP$^+$) and non-MGE population at E13.5 (EGFP$^-$). Statistical significance was set at $P < 0.01$.

Results

Conditional Loss of Function of Dicer in MGE-Derived Interneurons

Ventrally born cINs undergo 3 main transitions to reach their final positions in the dorsal telencephalon. First, cells exit the cell cycle and start migrating tangentially into the cortex; second, neurons switch from tangential to radial migration upon entering the CP; and finally, cells stop radial migration and undergo differentiation and specification. We reasoned that miRNA regulation might be central for these transition stages by fine-tuning gene expression. To specifically test this hypothesis in MGE-derived cINs, we crossed *Nkx2.1*^{Cre} (Xu et al. 2008) and *Lhx6*^{Cre} (Fogarty et al. 2007) transgenic mouse lines, with a mouse line carrying a conditional allele for *Dicer* (*Dicer*^{C}). This genetic strategy allows for the ablation of the fourth exon of the second RNAseIII domain of *Dicer* in Cre-expressing cells (Harfe et al. 2005) (Fig. 1*A*). The Nkx2.1 transcription factor is expressed exclusively within the ventricular and subventricular zones (VZ and SVZ, respectively) of the MGE. *Lhx6* expression is transcriptionally regulated by *Nkx2.1* and is initiated only when cells exit the VZ/SVZ progenitor regions and become postmitotic. As a result, *Lhx6* expression is largely excluded from proliferating cells. By using the *Nkx2.1*^{Cre} or *Lhx6*^{Cre} drivers, we were able to restrict the removal of *Dicer* to within the same population (MGE-derived cINs) but at

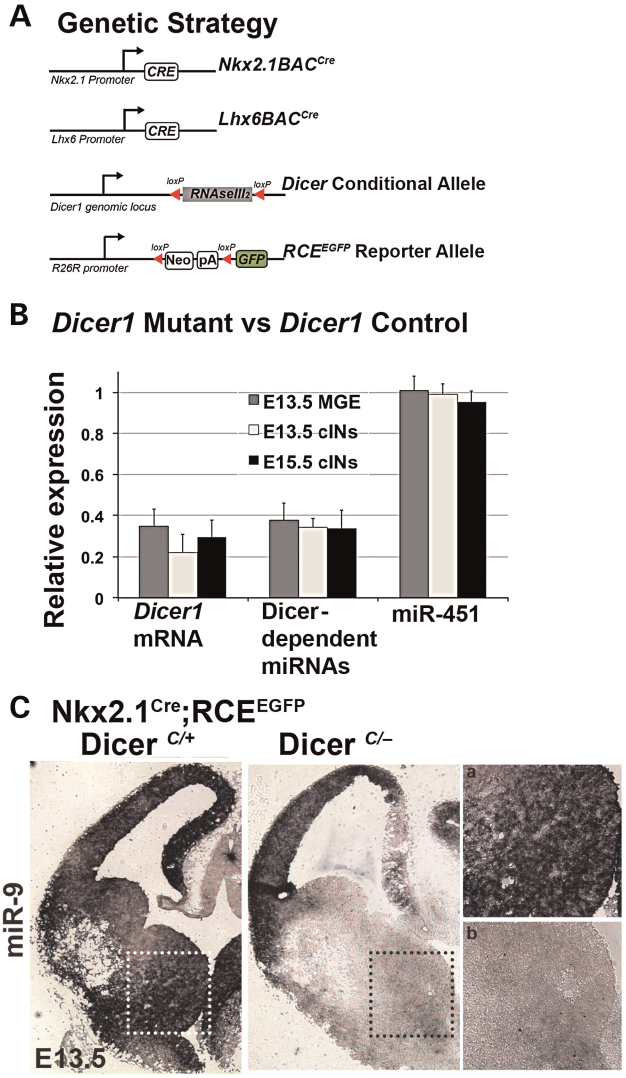

Figure 1. Conditional removal of *Dicer* in MGE-derived cortical interneurons. (*A*) A schematic showing conditional removal of *Dicer* within the MGE progenitor domain by using the *Nkx2.1*^{Cre} transgenic driver line or in postmitotic MGE-derived cINs by using the *Lhx6*^{Cre} driver line. *Nkx2.1*^{Cre} or *Lhx6*^{Cre} transgenic mice was crossed to a previously characterized *Dicer* conditional allele in which the loxP sites were inserted around the exon that encodes most of the second RNAseIII domain to eliminate *Dicer* function in MGE-derived cINs. We used the reporter allele RCE^{EGFP} to fate-mapped MGE-derived cells in the mutant and control animals. (*B*) Expression of *Dicer* mRNA and mature miRNAs in EGFP$^+$ cells isolated from E13.5 MGE, E13.5 cortex or E15.5 cortex of control (*Dicer*$^{F/+}$; *Nkx2.1*^{Cre}, *RCE*^{EGFP}) and mutant (*Dicer*$^{C/-}$; *Nkx2.1*^{Cre}, *RCE*^{EGFP}) animals analyzed by qRT-PCR. *GAPDH* and *U6* RNA were used as internal controls for Dicer mRNA and mature miRNA expression, respectively. Data are represented as the percent FC in miRNA expression in mutants normalized to control levels according to the Livak ($2^{-\Delta\Delta Ct}$) quantification method. Data represent mean ± SEM, $P < 0.01$ for all comparisons of mutant versus controls across all ages analyzed. (*C*) ISH of neural enriched miRNA-9 at E13.5 shows that mutant animals (*Dicer*$^{C/-}$; *Nkx2.1*^{Cre}, *RCE*^{EGFP}) have a dramatic reduction in Dicer1 activity within the MGE domain relative to control animals (*Dicer*$^{F/+}$; *Nkx2.1*^{Cre}, *RCE*^{EGFP}).

sequential time points. We used the reporter allele RCE^{EGFP}; (Sousa et al. 2009) to label *Nxk2.1*- and *Lhx6*-expressing cells with EGFP (Fig. 1*A*). This genetic strategy allowed us to address the role of miRNAs in mitotic versus postmitotic MGE-derived cINs, while tracking cells at different developmental time points using genetic fate mapping.

To confirm the efficacy of our genetic strategy, we compared the expression of *Dicer* mRNA and mature miRNAs by quantitative RT-PCR in *Dicer* conditional mutant embryos ($Dicer^{C/-}$; $Nkx2.1^{Cre}$; RCE^{EGFP}) versus controls ($Dicer^{C/+}$; $Nkx2.1^{Cre}$; RCE^{EGFP}) (Fig. 1*B*). We isolated MGE-derived INs in controls and mutants by FAC sorting EGFP-expressing cells from the MGE of E13.5 embryos, and the cortex of E13.5 and E15.5 embryos. To normalize *Dicer* mRNA and mature miRNA expression, we used *GAPDH* and *U6* RNA as internal controls. By using primers specific to the floxed exon of *Dicer* gene, we found that the *Dicer* mRNA levels in the EGFP-positive cells isolated from the MGE of E13.5 mutant animals was strongly reduced when compared with control embryos (65% reduction in mutants relative to controls). Furthermore, *Dicer* mRNA levels remained at low levels in mutant INs purified from the cortices of E13.5 (78% reduction) and E15.5 (70% reduction) embryos compared with controls. Consistent with the reduction of *Dicer* transcript, the expression of mature miRNAs was also significantly reduced in *Dicer* mutants relative to controls in the MGE of E13.5 and the cortices of E13.5 and E15.5 animals (Fig. 1*B*, Supplementary Table 1). As expected, we did not observe any changes in miR-451 expression levels in EGFP-positive cells at any time point during our analysis, which is independent of the canonical Dicer-mediated miRNA biogenesis pathway (Cheloufi et al. 2010). To confirm that *Dicer* activity is removed within the targeted conditional loss-of-function populations, we performed ISH of miR-9 and showed that miR-9 expression is completely removed from the VZ-MGE of mutant embryos at E13.5, while persisting within the dorsal cortex (Fig. 1*C*, Supplementary Fig. 1). Although, $Nkx2.1^{Cre}$ driver appears to be efficient in abrogating miR-9 from mutant cIN progenitors as early as E13.5, the persistent low levels *Dicer* mRNA and miRNAs detected by PCR suggests that our results reflects a hypomorphic rather than a null Dicer loss of function phenotype. Nonetheless, we found that remaining the *Dicer* mRNA and miRNA expression detected by PCR was not significantly different in mutant progenitor cells at E13.5 compared with mutant postmitotic neurons at E15.5 (Fig. 1*B*). Hence, by confining analysis to fate-mapped mutant and wild-type MGE-cINs within E13.5 progenitor zones and E15.5 migratory zones, we believe that this finding does not significantly skew our analysis of *Dicer* ablation at these distinct developmental stages.

Loss of Dicer in Nkx2.1-Expressing Cells Results in a Reduction in the Number of cINs

Inactivation of Dicer using the $Nkx2.1^{Cre}$ driver resulted in postnatally viable mice with smaller body weight compared with littermate controls and a slight reduction in brain size. Dicer mutant animals did not thrive after weaning and subsequently died between ages P23–P25. Visual examination indicated that Dicer mutant animals displayed handling-induced hyperexcitability and behavioral abnormalities that closely resembled epileptic encephalopathies previously observed in mice with MGE-derived cortical interneuron deficits (Butt et al. 2008; Batista-Brito et al. 2009; Close et al. 2012).

To investigate the consequences of *Dicer* removal in MGE-derived interneurons, we first examined the postnatal somatosensory cortex at P21. The laminar and topographic organization of the somatosensory cortices of $Dicer^{C/-}$; $Nkx2.1^{Cre}$; RCE^{EGFP} mutant animals were broadly normal as indicated by their proper lamination, as accessed by DAPI nucleic acid staining and by their proper expression of laminar markers such as Tbr1 and Ctip2 (data not shown). However, the genetic fate-mapping analysis of $Dicer^{C/-}$; $Nkx2.1^{Cre}$, RCE^{EGFP} mutant animals revealed gross deficits in the number of cINs (Fig. 2*A–C*). We found a significant reduction of cells expressing *Gad67* in $Dicer^{C/-}$; $Nkx2.1^{Cre}$, RCE^{EGFP} mutant animals relative to $Dicer^{C/+}$; $Nkx2.1^{Cre}$, RCE^{EGFP} control animals (20 ± 2% decrease in mutants) (Fig. 2*D*), particularly within the deep layers of analyzed mutant cortices (35 ± 1% decrease in mutants). To specifically label MGE-derived cINs, we analyzed *Lhx6* expression by ISH (Liodis et al. 2007). Consistent with the reduction in *Gad67* expression in Dicer mutant cINs, we observed a pronounced decrease in the number of cells expressing *Lhx6*, with a similar bias in cell reduction toward deep layers (Fig. 2*B*,*E*). To investigate whether the decrease in *Gad67* and *Lhx6* expression in mutant brains was a result of loss of cINs carrying Dicer mutation, we quantified the number of fate-mapped MGE-derived cINs by counting the number of cells expressing EGFP in comparable areas of control and mutant cortices (Fig. 2*C*,*F*). In mutant mice, the number of EGFP-positive MGE-derived cINs was decreased by 56 ± 5% compared with controls. In this regard, it is important to recognize that the expression of $Nkx2.1^{Cre}$ transgene does not fully recapitulate the wild-type expression of *Nkx2.1*, and is confined to ~70% of MGE-derived cINs (Xu et al. 2008), with a bias toward deep layers of the somatosensory cortex (see Fig. 3). As MGE-derived cINs comprise 70% of all cortical INs, the observed 56% decrease in the fate-mapped $Nkx2.1^{Cre}$ lineage is consistent with a 35% reduction in the observed total number of deep layer *Gad67*-positive INs. This suggests that the decreased number of cortical INs corresponds to the reduced number of MGE-derived cortical *Gad67* cells.

The loss of *Dicer* appears to also affect the development of MGE-derived cINs that persist in mutant animals. We observed that cINs in $Dicer^{C/-}$; $Nkx2.1^{Cre}$;RCE^{EGFP} mutant animals have morphological defects by P21, including both larger cell bodies and thicker dendrites with reduced branching of their apical processes compared with controls (Fig. 2*G*).

Dicer Mutant MGE Interneurons Retain Their GABAergic Fate but Fail to Express Interneuron Subtype Markers

Consistent with their MGE origin (Miyoshi et al. 2007), EGFP-expressing cells in $Dicer^{C/+}$; $Nkx2.1^{Cre}$; RCE^{EGFP} control animals predominantly co-labeled with either PV (Fig. 3*A*,*C*) or SST (Fig. 3*B*,*D*). However, the loss of miRNAs in MGE-derived cINs affected the expression of these mature markers within the mutant population. In mutants, the percentage of EGFP cells that express PV was 54 ± 4% reduced compared with controls (Fig. 3*C*). Similarly, we observed that the percentage of SST-expressing EGFP neurons was 36 ± 7% reduced compared with littermate controls (Fig. 3*D*). These results show that in addition to a decreased number of EGFP-positive neurons within the $Nkx2.1^{Cre}$-expressing population, the loss of miRNAs further disrupts the expression of MGE-derived cIN subtype markers. Nonetheless, mutant cINs that did not express the subtype markers PV or SST were still GABAergic as

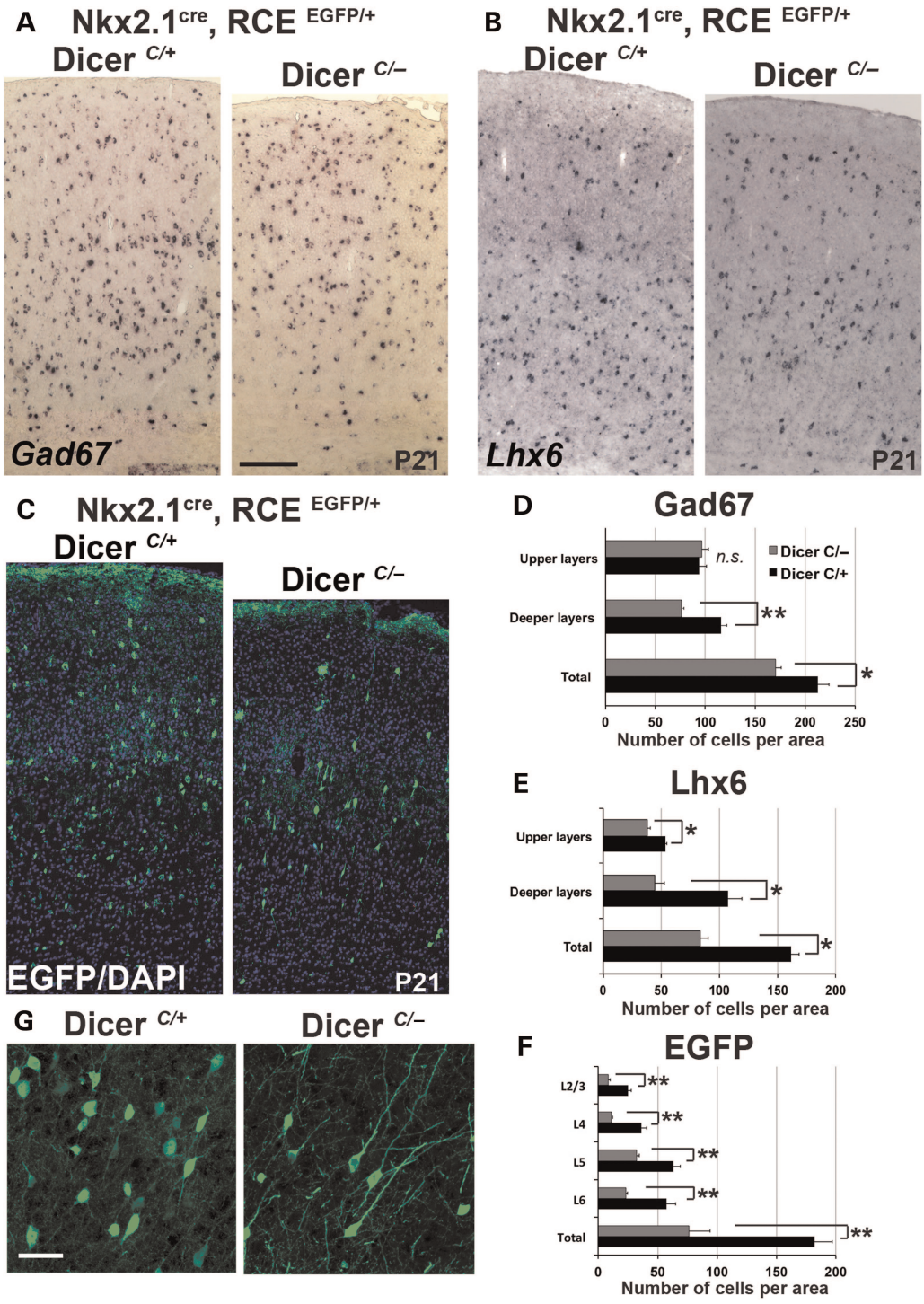

Figure 2. Loss of *Dicer* in MGE progenitor domain results in reduced number of MGE-derived cINs with severe morphological defects in the adult cortex. A pronounced reduction of the total number of cINS in the mutant brains compared with controls within the somatosensory cortex at P21. (*A*) ISH of *Gad67*, pan-interneuron marker, shows that mutant animals (*Dicer*$^{C/-}$; *Nkx2.1*^{Cre}, *RCE*^{EGFP}) have reduced number of cortical GABAergic neurons relative to control animals (*Dicer*$^{C/+}$; *Nkx2.1*^{Cre}, *RCE*^{EGFP}). The reduction in the number of *Gad67*-expressing cells in the cortex through cortical layers 2–6 is 20 ± 2%, and the percentage of decrease of the number of *Gad67*-expressing cells in deep layers is 35 ± 1%. Scale bar corresponds to 100 μm. Note that the *Dicer* mutant animals show a slight reduction in the brain size. (*B*) ISH of *Lhx6* shows reduced numbers of MGE-derived cINs, mostly in the deep layers (61 ± 5%). (*C*) Fate mapping of MGE-derived interneurons at P21 shows that the total number of EGFP-immunolabeled interneurons in the P21 cortex is reduced by 56 ± 5%. (*D*) Total number of *Gad67*$^{+}$ cells per optical field, control in black bars (213 ± 11) versus mutant in gray bars (170 ± 6), $n = 3$, $P < 0.05$. Cortex was divided into upper and deeper layers based on the density of cells among layers; upper layers: control (94 ± 8) versus mutant (97 ± 7), $P = 0.4$; deeper layers: control (116 ± 5) versus mutant (76 ± 3), $P < 0.01$. (*E*) Quantification of Lhx6^{+} cell numbers per optical field in control (161 ± 7) versus mutant (84 ± 7), upper layers: control (54 ± 1) versus mutant (38 ± 3), deeper layers: control (107 ± 12) versus mutant (45 ± 8), $n = 3$, $P < 0.05$ for all values. (*F*) The total number of cells expressing EGFP per optical field in the control (182 ± 15) versus mutant (76 ± 18), L2/3: control (25 ± 3) versus mutant (9 ± 2); L4: control (37 ± 5) versus mutant (12 ± 1); L5: control (63 ± 6) versus mutant (33 ± 2); L6: control (57 ± 8) versus mutant (23 ± 2), $n = 5$. Data represent mean ± SEM. *$P < 0.05$, **$P < 0.01$. (*G*) Confocal images from *Dicer*$^{C/-}$; *Nkx2.1*^{Cre}, *RCE*^{EGFP} mutant cortex layer 5 neurons (right panel) at P21 compared with controls (left panel) within layer 5 displays morphological defects in Dicer-depleted cINs. Pia is located toward the right corner of the image; scale bar corresponds to 20 μm.

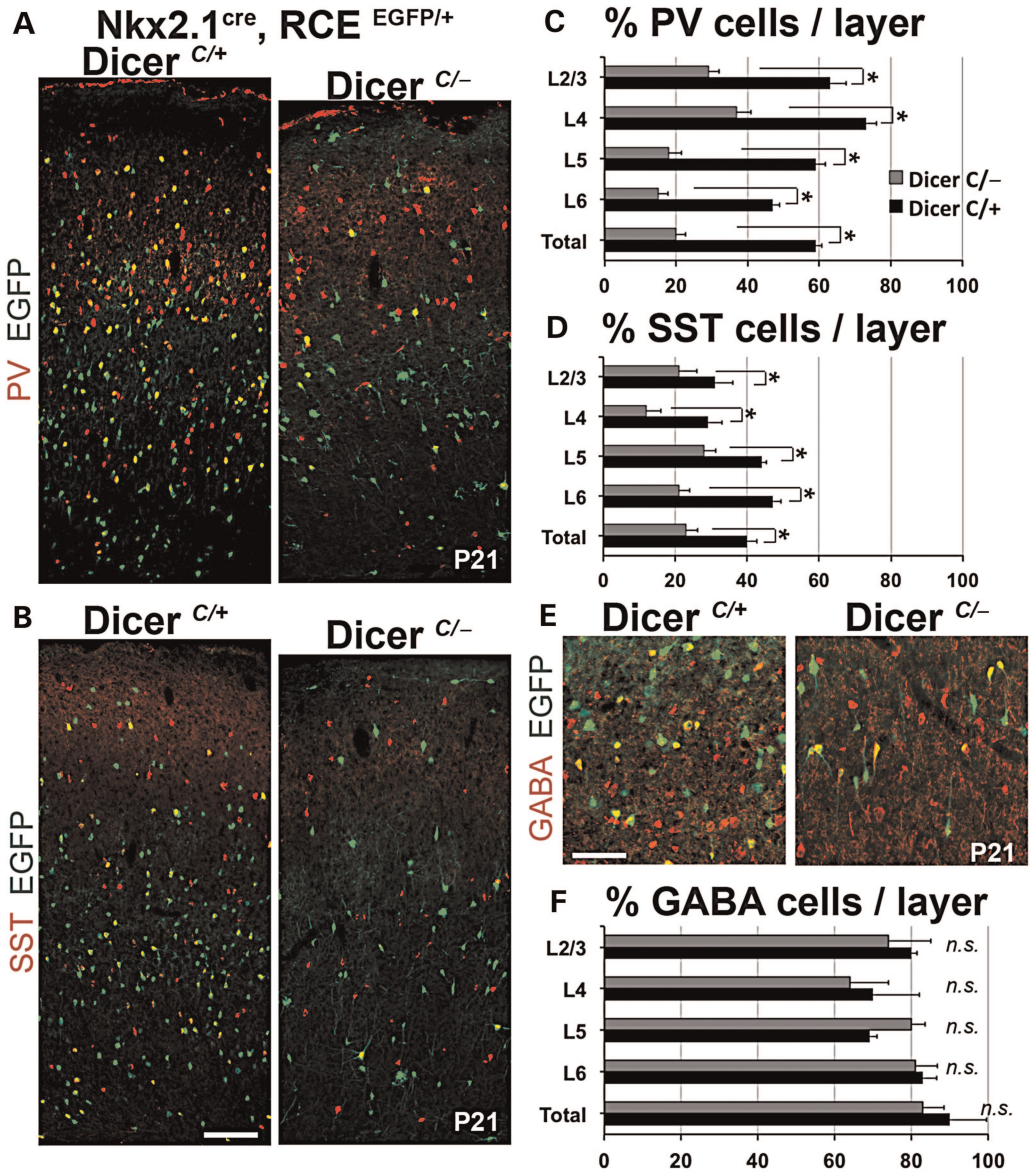

Figure 3. *Dicer* mutant MGE-derived cINs fail to express markers of their mature identity but retain their GABAergic fate. Effects of loss of miRNAs on cIN maturation at P21. (*A*) Subtype-specific cortical interneuron gene expression is assessed by double immunostainings for EGFP and parvalbumin (PV) and (*B*) somatostatin (SST) molecular markers. The percentage of fate-mapped cells in cortical layers 2–6 expressing PV and SST, relative to the total number of EGFP-positive neurons within all layers are significantly reduced in Dicer mutant brains (gray bars) compared with littermate controls (black bars). (*C*) The percentage of fate-mapped cells expressing PV per optical field: L2–6: control (59 ± 2%) versus mutant (20 ± 3%), L2/3: control (63 ± 5%) versus mutant (29 ± 3%); L4: control (73 ± 3%) versus mutant (37 ± 4%); L5: control (59 ± 3%) versus mutant (18 ± 4%); L6: control (47 ± 2%) versus mutant (15 ± 3%), $n = 5$, $P < 0.01$ for all values. (*D*) The percentage of fate-mapped cells expressing SST per optical field: L2–6: control (40 ± 3%) versus mutant (23 ± 3%), L2/3: control (31 ± 5%) versus mutant (21 ± 5%); L4: control (29 ± 4%) versus mutant (12 ± 4%); L5: control (44 ± 2%) versus mutant (28 ± 3%); L6: control (47 ± 3%) versus mutant (21 ± 3%), $n = 4$, $P < 0.01$ for all values. (*E*) Removal of *Dicer* from fate-mapped neurons does not affect their GABAergic identity. (*F*) The percentage of fate-mapped cells expressing GABA per optical field: L2–6: control (90 ± 10%) versus mutant (83 ± 6%), L2/3: control (80 ± 2%) versus mutant (74 ± 11%); L4: control (70 ± 12%) versus mutant (64 ± 10%); L5: control (69 ± 2%) versus mutant (80 ± 4%); L6: control (83 ± 4%) versus mutant (81 ± 6%), $n = 4$, $P > 0.5$ for all values. Data represent mean ± SEM. Scale bars in (*B*) and (*E*) correspond to 100 and 40 μm, respectively.

indicated by the unaltered colocalization of EGFP and GABA in mutants relative to controls (Fig. 3*E*,*F*). These data suggest that the loss of *Dicer* disturbs the specific subtype marker expression of MGE-derived cINs but not their GABAergic identity. To exclude the possibility that mutant cINs underwent a subtype fate switch, we verified that mutant cINs did not express markers characteristic of CGE-derived cINs (Lee et al. 2010) (data not shown). Taken together, our results demonstrated that removal of Dicer from the MGE progenitor domain cell autonomously reduces the number of MGE-derived cINs, leads to the loss of their mature molecular subtype markers and disrupts their morphological characteristics by P21.

The Reduced Number of Mature MGE-Derived Cortical Interneurons is Not Due to Proliferation Defects

The reduction in MGE-derived cIN number upon *Dicer* ablation might be due to either a decrease in the number of neurons generated from this progenitor domain, a loss of neurons by cell death or a combination of both factors. To discern the underlying cause of cellular phenotypes observed

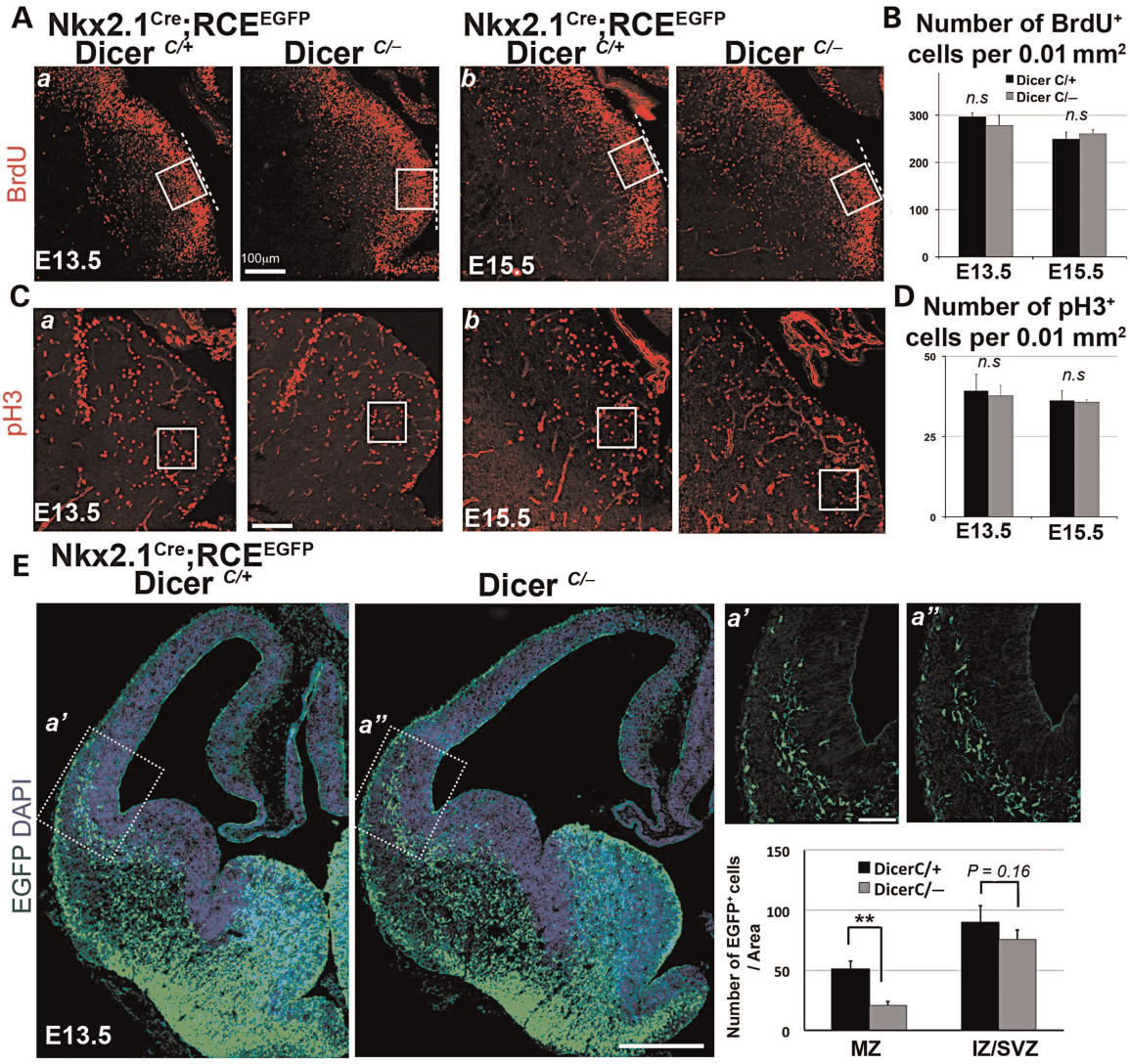

Figure 4. The reduced number of mature MGE-derived cINs is not due to a decrease in number of progenitors, nor to changes in the cell cycle. The effects of *Dicer* removal in the fate-mapped MGE-derived INs were examined using immunofluorescence analysis of proliferation of MGE progenitors in coronal sections from E13.5 and E15.5 control and mutant Dicer animals. (*A*) BrdU (1 mg BrdU per 10 g of body weight, intraperitoneal, 1 h before fixation), incorporated during S phase shown in panels a and b correspond to E13.5 and E15.5, respectively. The dashed lines are included to ensure accurate positioning of the MGE with respect to the ventricles. (*B*) Density of $BrdU^+$profiles per 0.01-mm^2 region within the MGE was similar in mutant and control embryos at both E13.5 (278 ± 13 vs. 296 ± 8, $n = 3$, $P = 0.379$) and E15.5 (261 ± 5 vs. 249 ± 15, $n = 3$, $P = 0.554$). (*C*) Immunofluorescence analysis of pH3, M phase marker in E13.5 (a) and E15.5 (b) coronal sections. (*D*) Number of $pH3^+$ profiles per 0.01-mm^2 areal density within MGE was similar in mutant and control embryos at both E13.5 (37.6 ± 3.3 vs. 39.2 ± 5.2, $n = 3$, $P = 0.815$) and E15.5 (35.8 ± 0.8 vs. 36.2 ± 3.1, $n = 3$, $P = 0.884$). (*E*) $EGFP^+$ fate-mapped cells within the subpallial regions do not display overt differences in mutants compared with controls. *Dicer* mutant cINs are capable of initiating tangential migration and enter dorsal telencephalon following 2 migratory routes (arrows, MZ, upper and IZ/SVZ, lower migratory zones). However, in comparison to littermate controls (Ea′), Dicer mutant MGE-derived cINs showed mild reduction in the leading edge of tangentially migrating INs in both superficial and deep migratory zones (Ea″). (*F*) The number of fate-mapped cINs in controls compared with mutant MGE-derived cINs within MZ (50 ± 7 vs. 21 ± 6, $n = 6$, $P < 0.01$) and IZ/SVZ (90 ± 15 vs. 76 ± 8, $n = 6$, $P = 0.16$) migratory zones at E13.5. Data represent mean ± SEM, $^*P < 0.05$, $^{**}P < 0.01$. Scale bar corresponds to 100 μm in A, C, Ea′, Ea″, 500 μm in E.

in *Dicer* mutant cINs in mature cortices, we focused our analysis on fate-mapped MGE-derived lineage during progressive stages of embryonic development.

Recent studies demonstrate that miRNAs are important for proliferation and maintenance of different types of neuronal progenitors (Makeyev et al. 2007; Choi et al. 2008; De Pietri Tonelli et al. 2008), but little is known about how they affect cIN progenitors. We investigated whether the loss of *Dicer* results in impaired proliferation of the MGE by analyzing their S phase through examination of the incorporation of BrdU in the MGE of control and mutant embryos (Fig. 4*A*). One-hour BrdU pulse labeling at E13.5 and E15.5 demonstrated that the number of cells in S phase was not significantly altered in mutants relative to controls (Fig. 4*B*). Moreover, we noted that the size of the MGE per se in Dicer mutants and controls in anatomically matched embryonic coronal sections is indistinguishable. Next, we analyzed the number of mitotic cells in controls versus mutants by immunofluorescence labeling for phosphorylated histone H3 (PH3), which specifically labels cells in the M-phase of cell cycle (Fig. 4*C*). Both at E13.5 and at E15.5, the number of mitotic cells was not significantly altered in mutants compared with controls (Fig. 4*D*). These results demonstrate that reduced levels of Dicer activity and decreased expression of mature miRNAs in *Nkx2.1*^{Cre} expressing

progenitor domain does not influence cell proliferation or alter cell cycle dynamics of the MGE progenitor niche.

Loss of miRNAs Resulted in Migratory Defects in MGE Interneurons Within the Cortical Plate

Although MGE-specific *Dicer* mutant embryos appeared grossly normal within the subpallial domains, we observed defects in MGE-derived cINs as they migrate past the subpallial–pallial boundary and reach the developing CP (Fig. 4*E*). Cortical INs enter the dorsal telencephalon through 2 different tangential migratory routes: A superficial path within the marginal zone (MZ); and a deep route positioned at the intermediate zone (IZ)/SVZ interface (Lavdas et al. 1999). To acquire their final position within appropriate cortical layers, cINs transit from tangential to radial migration (Marin and Rubenstein 2001). *Dicer* mutant MGE-derived cINs were able to tangentially migrate into the cortex via both the MZ and IZ/SZV routes (arrows in Fig. 4*E*). However, once they enter the dorsal pallium at E13.5, *Dicer* mutant cINs (Fig. 4*Ea″*) display defects predominantly within the MZ superficial migratory path. We observed that the number of mutant cINs within the MZ migratory path was 58 ± 4% reduced compared with controls (Fig. 4*F*, $P < 0.05$). Nonetheless, there was only a mild reduction (15 ± 6%), in the number of mutant cINs migrating within the IZ/SVZ of mutants compared with controls ($P = 0.16$).

We next analyzed the migratory behavior of *Dicer* mutant MGE-derived cINs at later stages of embryonic development, as cINs radially integrate into different cortical layers (Fig. 5). To identify specific cortical laminae, we used DAPI nuclear staining and the transcription factor Tbr1, which at perinatal ages is expressed in subplate, layer 6, and at lower levels in layer 5 (Hevner et al. 2001). We compared the number of fate-mapped neurons within the CP compared with the MZ and IZ/SVZ, within mutant versus controls embryos at E15.5 and E18.5 (Fig. 5*A–D*). Consistent with a reduction in mutant MGE-derived cINs tangentially migrating via the MZ path at E13.5, E15.5 mutants had a robust decrease in the number of neurons within the MZ (45 ± 4%), but a milder reduction within the CP (16 ± 4%) and IZ/SVZ (18 ± 4%) zones, respectively. Specifically within the IZ/SVZ migratory zone, mutant EGFP-expressing cells appeared abnormally clustered together when compared with control EGFP cells within the same region (arrowheads in Fig. 5*A*,*B*).

By E18.5, the time when the majority of wild-type MGE-derived cINs have switched to a radial mode to enter the CP (Miyoshi and Fishell 2011), we observed a robust reduction in the number of $EGFP^+$ cells in both the CP (60 ± 2%) and MZ regions (36 ± 7%, Fig. 5*F*) of mutant embryos. At this stage, the number of mutant $EGFP^+$ cells in the SVZ/IZ lower migratory zone was also decreased by 22 ± 3%. These results indicate a gradual reduction in the number of Dicer-deficient cINs both within the migratory zones as well as within the CP from E15.5 to E18.5. Such gradual depletion of $EGFP^+$ cells is apparent when the relative layer positions of MGE-derived cINs at E15.5 and E18.5 are considered (Fig. 5*E*,*F*). The percent reduction in the number of *Dicer* mutant cells in the MZ and IZ/SVZ were similar at both ages. However, the reduction of *Dicer* mutant cINs in the CP was much more dramatic by E18.5, as indicated by the 60 ± 2% decrease in E18.5 versus the 16 ± 4% decrease observed in E15.5 embryos. These results suggest that *Dicer* mutant cINs have difficulty entering the CP. Notably, the postmitotic removal of *Dicer* (mediated by the $Lhx6^{cre}$ driver) results in a similar, albeit milder, phenotype (31 ± 4% reduction in CP at E18.5 compared with 17 ± 4% reduction at E15.5; Fig. 5*G–J*). Hence, irrespective of the driver used to abolish Dicer function, we observed a dramatic and progressive reduction of cINs within the CP.

Loss of miRNAs Increases Apoptosis and Causes a Reduction of Postmitotic MGE-Derived Interneurons

Next, we investigated the underlying cause of the reduction in the number of Dicer-deficient MGE-derived cINs. The absence of any detectable change in the proliferation or accumulations of mutant cells within the migratory zones, lead us to hypothesize that cell loss is due to increased programmed cell death in mutants. In fact, a number of studies have demonstrated antiapoptotic roles for miRNAs during neuronal development (Karres et al. 2007; Kim et al. 2007; Schaefer et al. 2007; Davis et al. 2008; De Pietri Tonelli et al. 2008). To test for apoptosis, we performed immunohistochemistry for the cleaved (active) form of caspase-3. We did not observe a significant difference in caspase-3 signal within the MGE domain at E13.5 (Fig. 6*A*), suggesting that cell death is not occurring within progenitors at this age (Fig. 6*A*). In contrast, we observed increased caspase-3 expression in the MGE-ventricular region, as well as within the cortex of E15.5 mutant embryos compared with controls (Fig. 6*B*). However, since the vast majority of MGE-derived cINs are born before E15.5 (Miyoshi et al. 2007; Inan et al. 2012), we inferred that programmed cell death within the migratory zones but not the ventricular zones accounts for the reduced number of MGE-derived cINs in the developing cortex. As PV expressing Chandelier cells are generated at later ages (Taniguchi et al. 2013), we cannot exclude the possibility that apoptosis of E15.5 MGE progenitors in mutant mice leads to a reduced number of PV Chandelier cells in the adult brain. We therefore focused our analysis within the cortices of E15.5 and E18.5 embryos, where we observed that the number of apoptotic MGE-derived cINs was increased in mutants compared with controls (Fig. 6*C–E*). In particular, the number of MGE-cINs colocalized with caspase-3 peaked within the IZ/SVZ migratory zone of E15.5 mutant embryos (Fig. 6*D*), and that the mean number of caspase-3-positive cINs did not further increase by E18.5 (Fig. 6*E*). Taken together, our results suggest that in the absence of Dicer activity, MGE-derived cINs appear to initiate apoptotic programs predominantly within the migratory zones of developing cortex and as a consequence fail to populate the CP. The neuronal cell loss that occurs in MGE-derived cINs could result from the requirement of miRNAs to suppress expression of proapoptotic factors. Alternatively, increased apoptosis might be secondary to the elimination of cells whose differentiation programs are altered as a result of miRNA ablation. To distinguish between these possibilities, we sought to determine which mRNAs and miRNAs that are selectively expressed within postmitotic MGE-derived cINs.

Apoptotic machinery and IN-subtype-specific genes are upregulated in Dicer mutant MGE-derived interneurons during development.

To identify the genetic programs that directly depend on miRNA machinery during MGE-derived cIN development, we used microarrays to examine changes in the mRNA profile

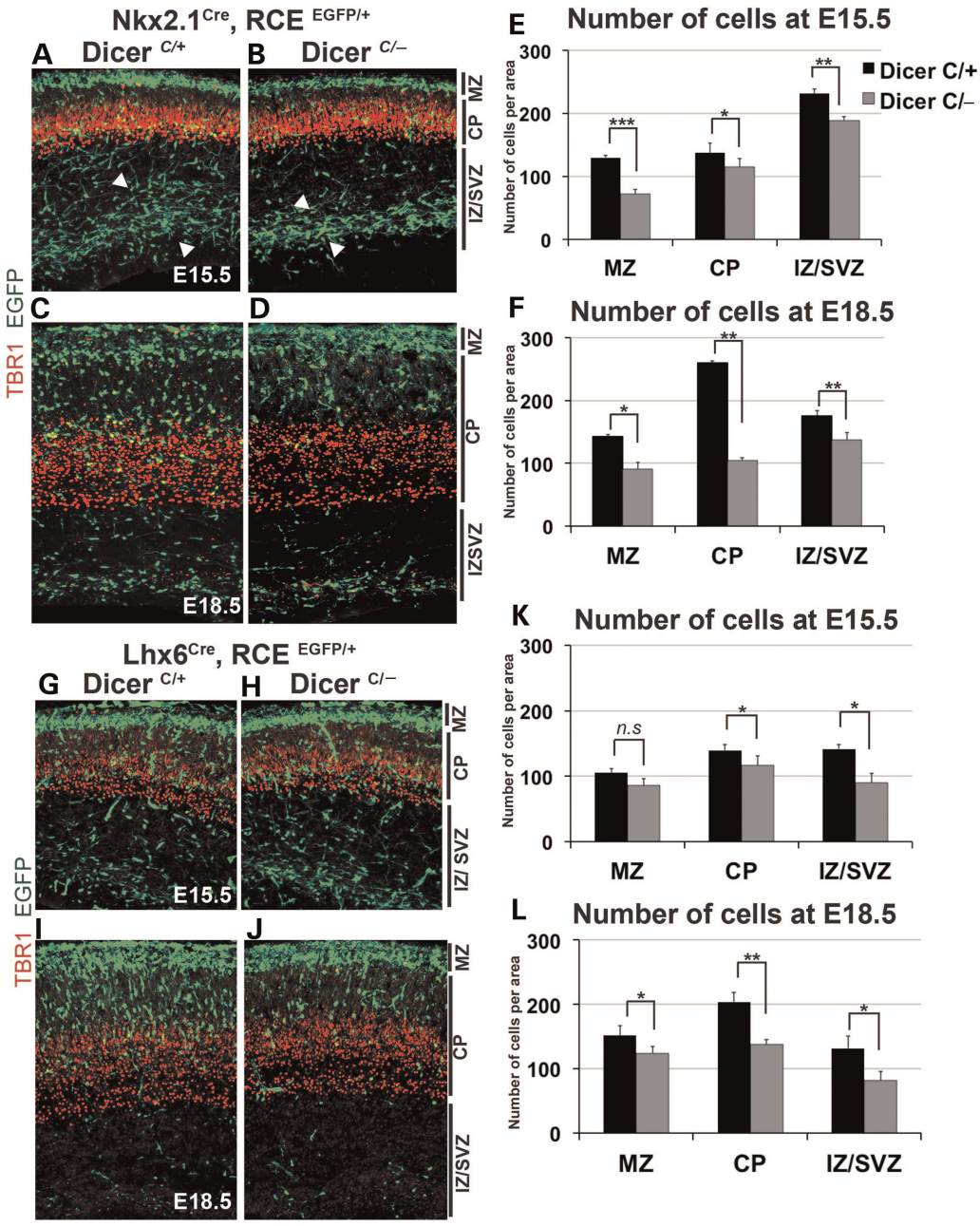

Figure 5. Loss of miRNAs in MGE-derived INs affects their migration into the CP. To determine if loss of *Dicer* affect interneuron migration, we fate-mapped control (*Dicer*$^{C/+}$; *Nkx2.1*^{Cre}; *RCE*$^{EGFP/+}$ or *Dicer* $^{C/+}$; *Lhx6*^{Cre}; *RCE*$^{EGFP/+}$ in A, C, G, I) and mutant interneurons (*Dicer*$^{C/-}$; *Nkx2.1*^{Cre}; *RCE*$^{EGFP/+}$ or *Dicer*$^{C/-}$*Lhx6*^{Cre}; *RCE*$^{EGFP/+}$ in B, D, H, J) during embryonic development. Embryonic cortical layers were visualized using Tbr1 (red) expressed in layers 5–6 and DAPI nuclear staining (not shown) for superficial layers. (*A* and *B*) The laminar distribution of control and mutant fate-mapped neurons at E15.5 shows that mutant animals have reduced number of cells in the MZ and clustered cells in the IZ/SVZ zones, while the number of cells within the CP is only slightly reduced. (*C* and *D*) The laminar distribution of mutant fate-mapped neurons at E18.5 shows a dramatic reduction in the number of cells in the CP, while the reduction in the MZ and IZ/SVZ migratory regions remained relatively similar between E15.5 and E18.5. (*E*) The number of cells per optical field at E15.5 in control (black) versus mutant (gray) embryos within the MZ (130 ± 4 vs. 72 ± 7, $P < 0.001$), CP (137 ± 15 vs. 115 ± 13, $P < 0.05$), and IZ/SVZ (231 ± 7 vs. 189 ± 6, $P < 0.01$), respectively. $N \geq 5$ embryos, with ≥3 sections analyzed per animal. (*F*) Total number of fate-mapped cells in E18.5 embryos in controls and mutants within MZ (142 ± 3 vs. 91 ± 11, $P < 0.05$), CP (259 ± 4 vs. 105 ± 4, $P < 0.01$), and IZ/SVZ (176 ± 8 vs. 137 ± 11, $P < 0.01$), respectively, $n \geq 3$ embryos, with ≥3 sections analyzed per animal. (*G* and *H*) At E15.5, conditional *Dicer* removal from postmitotic MGE-derived cINs with *Lhx6*^{Cre} driver leads to a reduction in the number of neurons within CP and SVZ/IZ. The milder phenotype observed in *Lhx6*^{Cre} removal of *Dicer* is likely due to later ablation of the gene than Nkx2.1^{Cre} driver. (*I* and *J*) At E18.5, the distribution of mutant fate-mapped neurons is altered. The number of cells in CP is further reduced relative to the E15.5 embryos, while the reduction MZ and IZ/SVZ layers remained relatively constant across the 2 developmental ages. (*K*) The number of fate-mapped control (black) and mutant (gray) neurons at E15.5 in MZ (106 ± 6 vs. 86 ± 10, $P = 0.1$), CP (140 ± 9 vs. 117 ± 14, $P < 0.05$), and IZ/SVZ (142 ± 6 vs. 90 ± 14, $P < 0.05$) respectively, $n = 3$ embryos, with ≥3 sections analyzed per animal. (*K*) Total number of fate-mapped cells in E18.5 embryos in controls and mutants within MZ (152 ± 15 vs. 124 ± 10, $P < 0.05$), CP (204 ± 15 vs. 137 ± 8, $P < 0.01$), and IZ/SVZ (131 ± 19 vs. 82 ± 14, $P < 0.05$), respectively, $n = 3$ embryos, with ≥3 sections analyzed per animal. Data are represented as mean ± SEM, $^*P < 0.05$, $^{**}P < 0.01$, $^{***}P < 0.001$. Scale bar in (*B*) corresponds to 200 μm in A, G, and H and 150 μm in C, D, I, and J.

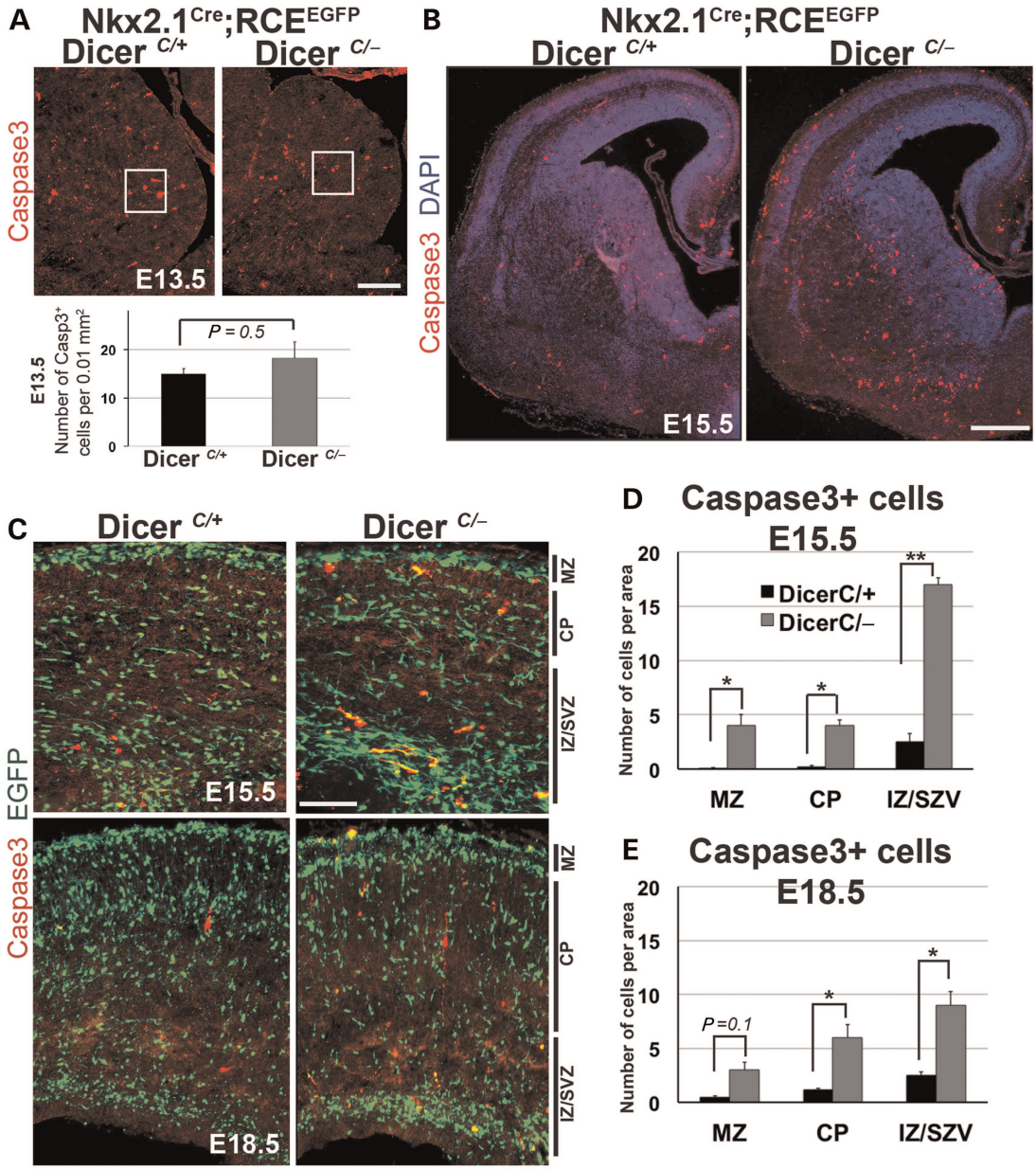

Figure 6. Loss of miRNAs in MGE-derived INs results in increased cell death and a progressive reduction of these cINs. Cell death in *Dicer* mutant MGE-derived cINs was assessed by the expression of the apoptotic marker caspase-3. (*A*) Caspase-3^{+} profiles per 0.01-mm^2 areal density within MGE was similar in mutant and control embryos at E13.5 (15 ± 1 vs. 18 ± 4 per 0.0-mm^2 areal density, $n = 3$, $P = 0.502$) (*B*) Increased expression of caspase-3 was observed at E15.5 in mutant brains compared with controls once MGE-derived cINs become postmitotic and migratory. (*C*) Upregulation of caspase-3 in *Dicer* mutant embryos is largely confined to MGE-derived cINs (EGFP) within the cortex at E15.5 (upper panels), and E18.5 (lower panels), as indicated by the progressive loss of genetically fate-mapped cells. (*D*) The number of EGFP/caspase-3 double-positive neurons in control versus mutants at E15.5 within MZ (0.1 ± 0.1 vs. 4 ± 1, $P < 0.05$), CP (0.2 ± 0.1 vs. 4 ± 0.5, $P < 0.05$), and IZ/SVZ (2.5 ± 0.6 vs. 17 ± 0.8, $P < 0.01$). (*E*) By E18.5, there is a reduced fraction of cINs undergoing cell death as assayed by EGFP/caspase-3 double-positive controls versus mutants within MZ (0.5 ± 0.1 vs. 3 ± 0.7, $P = 0.11$), CP (1.2 ± 0.1 vs. 6 ± 1.2, $P < 0.05$), and IZ/SVZ (2.5 ± 0.3 vs. 9 ± 1.3. $n = 3$, $P < 0.05$), respectively, $n = 3$ embryos, with ≥3 sections analyzed per animal. Data are represented as mean ± SEM, $^*P < 0.05$, $^{**}P < 0.01$. Scale bars corresponds to 100 μm in A, 500 μm in B, and 200 μm in upper panels of C and 150 μm in lower panels of C.

specifically in MGE-derived EGFP-positive cells in mutants (*Dicer*$^{C/-}$; *Nkx2.1*^{Cre};*RCE*^{EGFP}) compared with controls (*Dicer*$^{C/+}$; *Nkx2.1*^{Cre};*RCE*^{EGFP}) at E15.5 (Fig. 7*A*). We performed gene expression analysis on cells isolated from E15.5 cortices, since this was the earliest developmental time point when we observed a robust phenotype in Dicer mutants. We have purified MGE-derived cINs from cortex of mutant and control embryos by FAC sorting, and the total RNA isolated (100 ng, mutant = 3, control = 3) was amplified, labeled, and hybridized onto Affymetrix microarrays (MOE430v2), containing 45 000 probe sets (Cammenga et al. 2003; Rajasekhar et al. 2003; Batista-Brito et al. 2008). We extracted the microarray data using GeneSpring GX 10 software and used a threshold of >100 on the raw signal intensity values, resulting in 11 198 probe sets, which were then subjected to statistical analysis by comparing raw signal intensities between mutant and control gene-chips (FC ≥2, $P < 0.01$). Mammalian miRNAs are predominantly negative regulators of gene expression (Lewis et al. 2003). As anticipated from previous studies, our analysis revealed that 91 probe sets corresponding to 69 different Entrez gene

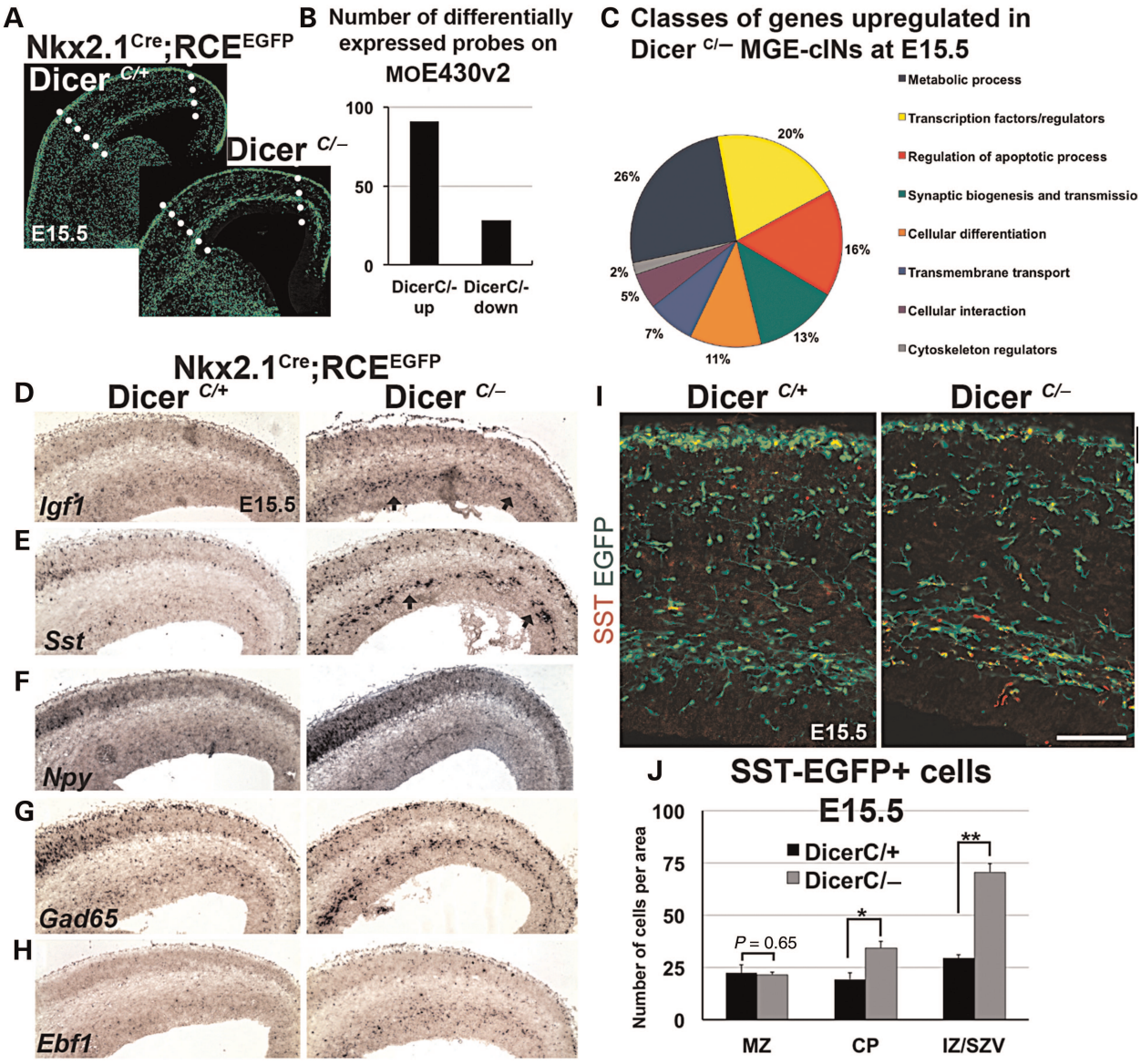

Figure 7. Identification of genes misregulated in the *Dicer* mutant MGE-derived cINs by mRNA microarray analysis. (*A*) RNA was extracted from FAC-sorted EGFP$^+$ INs (mutant = 3, control = 3), normalized and used to hybridize Affymetrix microarrays (MOE430v2). (*B*) Microarray data revealed that 91 probe sets corresponding to 69 different Entrez gene identifiers were enriched in the *Dicer* mutant MGE-derived INs compared with controls, whereas only 28 probe sets corresponding to 20 different mRNAs were downregulated. (*C*) Analysis of the Gene Ontology consortium terms of the upregulated genes (55 of 69 genes hold annotated biological function) shows genetic programs including metabolic process (14 of 55), transcription (11 of 55), regulation of apoptotic process (9 of 55), synaptic biogenesis and transmission (7 of 55), cellular differentiation (6 of 55), transmembrane transport (4 of 55), cellular interaction (3 of 55), and regulation of cytoskeleton (1 of 55) are deregulated in MGE-derived cINs in the absence of mature miRNAs. (*D–H*) ISH expression analysis of the survival gene *Igf1*, as well as interneuron maturation genes *Sst*, *Npy*, *Gad65*, and *Ebf1* as a validation of genes misregulated in the absence of *Dicer* mutants (right panels) compared with littermate controls (left panels) in the developing cortex. Note the expression pattern of these genes with an upregulation primarily within deeper migrator zones (arrows). (*I*) *Dicer* mutant fate-mapped cINs show cell-autonomous upregulation of SST specifically within IZ/SVZ. (*J*) The number of SST+EGFP double-positive neurons in controls versus mutants within MZ (22.4 ± 3.8 vs. 21.6 ± 1.1, $P = 0.65$), CP (19.3 ± 3 vs. 34.2 ± 3.3, $P < 0.05$), and IZ/SVZ (29.4 ± 1.7 vs. 70.6 ± 4.2, $P < 0.01$), respectively. $n = 3$ embryos, with ≥3 sections analyzed per animal. Data are represented as mean ± SEM, $^*P < 0.05$, $^{**}P < 0.01$. Scale bars corresponds to 100 μm in *I*.

identifiers were enriched (or upregulated) (FC ≥ 2) in the *Dicer* mutant cINs compared with controls, whereas only 28 probe sets corresponding to 20 different mRNAs were downregulated (FC ≥ 2) in the *Dicer* mutant cINs compared with controls (Fig. 7*B*, Supplemental Table 2). Analysis of the Gene Ontology consortium terms of the upregulated genes (Ashburner et al. 2000) in *Dicer*-ablated MGE-derived cINs revealed that a wide array of genetic programs are dysregulated (Fig. 7*C*). By classifying the genes with regard to their annotated biological function, we showed that upregulated genes within mutant embryos were, respectively, involved with metabolism (14 of 55 genes with annotated biological functions such as *Man1a*, *Crabp1*, *Ppm1a*, *B3gnt2*, *Pam*, *Ecel*); transcription (11 of 55: *magel2*, *Klf6*, *Nr1d2*, *Ebf1*, *Zfp503*, *Zfp386*); regulation of apoptosis (9 of 55: *igf1*, *Rreb1*, *Pde1*, *Jun*, *Prkcd*, *Bcl2l11*); synaptic biogenesis and transmission (7 of 55: *sst*, *Npy*, *Ddc*, *Gad2*, *Tac1*, *Clcn5q*); cellular differentiation (6 of 55: *pou3f4*, *Npnt*, *Dlk1*, *Meis1*); transmembrane transport (4 of 55: *slc25a24*, *Slc25a13*, *Vat1*); cellular interaction (3 of 55: *mbc2*, *Pcdh21*, *Cdh22*); and regulation of cytoskeleton (1 of 55;

Kif16b) (Supplementary Table 2, Fig. 7). Of these genes, *Igf1* showed the greatest fold enrichment in *Dicer* mutant MGE-derived cINs compared with controls (22.98 ± 7.68, Supplementary Table 2). *Igf1* has been widely studied for its role in neuronal survival (Ye and D'Ercole 2006; Llorens-Martin et al. 2009) and differentiation (Ozdinler and Macklis 2006). To our surprise, we also noticed a significant upregulation in the mRNA expression levels of genes that are expressed in mature cINs, namely *Sst*, *Npy*, *Gad2*, and *Tac1* (*Substance P*) (Batista-Brito et al. 2008) (Supplementary Table 2). In addition, *Ebf1* gene encoding the transcription factor required for differentiation and migration of lateral ganglionic eminence-driven striatal INs was also enriched in *Dicer*-deficient cINs (Supplementary Table 2) (Garel et al. 1999; Garcia-Dominguez et al. 2003).

To verify that the expression patterns of *Igf1*, *Sst*, *Npy*, *Gad65*, *Ebf1* were indeed altered, we performed ISH or immunohistochemistry on E15.5 mutant embryos and littermate controls (Fig. 7*D–I*). Consistent with our microarray analysis, ISH showed that the expression of *Igf1*, *Sst*, *Npy*, *Gad65*, and *Ebf1* were increased specifically in the IZ/SVZ migratory region of the mutant cortices (arrows in Fig. 7*D,E*). Through immunohistochemical analysis, we determined that EGFP-SST double-labeled neurons were far greater within the IZ/SVZ region of the mutants when compared with control embryos at E15.5 (Fig. 7*I,J*). In fact, upregulation of SST protein in IZ/SVZ was already visible at E13.5, before the onset of cell apoptotic cell death in MGE-cINs (Supplementary Fig. 2*A,B*). Taken together, our data suggest that, in the absence of miRNAs, MGE-derived cINs start expressing genes characteristic of their mature subtype identity precociously and have apoptotic programs abnormally triggered during development. Therefore, we conclude that miRNAs are crucial for the correct expression of cIN-specific genes as well as apoptotic genes, allowing INs to undergo their normal developmental programs.

miRNAs are Selectively Enriched in Postmitotic MGE-Derived Cortical Interneurons Compared with Progenitors

Based on previous studies, the changes in the mRNA profiles in MGE-derived cINs do not need to result from the miRNA interacting directly with the downregulated messages. The changes in mRNA levels may also result from the repression of key regulatory genes expressed specifically during translation or due to off-target effects of *Dicer* ablation (Farh et al. 2005; Lim et al. 2005; Bartel 2009). Thus, we sought to identify miRNAs that are selectively expressed in postmitotic MGE-derived cells within the cortex compared with proliferative cells within the MGE. For this purpose, we dissected out the MGE of *Nkx2.1*^{Cre}, *RCE*^{EGFP} embryos at E13.5, and the cortex of *Nkx2.1*^{Cre}, *RCE*^{EGFP} embryos at E15.5 (Fig. 8*A*), and FAC sorted the EGFP$^+$ cells. We also collected EGFP$^-$ cells during FAC sorting to compare miRNA expression levels in MGE-derived cells to those of non-MGE cells, which are largely comprised by glial progenitors within the MGE at E13.5, and proliferating and postmitotic excitatory projection neurons in the cortex by E15.5. Normalized levels of miRNA isolated from EGFP$^+$ and EGFP$^-$ cells from the 2 regions of interest were subjected to Agilent miRNA microarrays, containing 611 mouse mature miRNAS and 39 mouse viral miRNAs ($n = 3$ for E13.5-EGFP$^+$, E13.5-EGFP$^-$, E15.5 EGFP$^+$, and E15.5 EGFP$^-$). We have extracted the miRNA microarray data using GeneSpring GX 10 software. As the miRNAs with

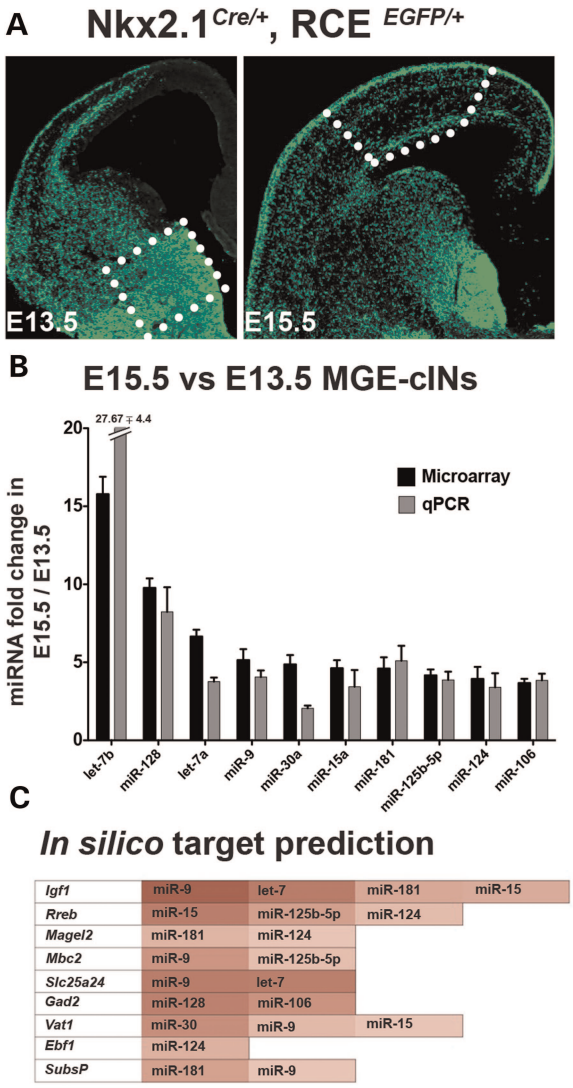

Figure 8. Selective upregulation of miRNAs in postmitotic MGE-derived cINs. Identification of temporally enriched miRNAs. (*A*) We used Agilent miRNA microarrays to compare the expression of miRNA between Nkx2.1 fate-mapped cells from the E13.5 proliferative MGE and Nkx2.1 fate-mapped cells that have migrated into the cortex at E15.5 (in triplicates). (*B*) Averaged FCs in the miRNA expression levels in migratory E15.5 INs relative to E13.5 proliferative cells as assessed by Agilent miRNA microarrays (black, $n = 3$) and Taqman qRT-PCR (gray, $n = 3$–4), from independently collected EGFP$^+$ cells. 3X independent runs per sample for qRT-PCR using *U6* RNA as internal control. Error bars show mean ± SEM. (*C*) *TargetScan*, *miRanda*, and *DIANA microT* prediction algorithms was used for the preliminary evaluation of targeting between mRNA transcripts that were upregulated in MGE-derived cINs devoid of the *Dicer* enzyme with miRNAs upregulated in migratory MGE-cINs. miRNAs were ranked based on the context score, darker colors correspond to higher scores predicted by *miRanda* algorithm.

higher expression levels seem likely to have greater biological impact on the cell expressing them, we considered miRNAs that have raw signal intensity values >100. When we applied this threshold to E13.5 EGFP$^+$ cells analyzed on affymetrix chips, 100 of 611 probes exceeded the raw signal intensity of 100, whereas 74 exceeded this threshold when EGFP$^-$ cell were analyzed. A similar comparison at E15.5 of EGFP$^+$ cells revealed that 137 exceeded this threshold, whereas, in age-matched EGFP$^-$ cells, 147 probes exceeded this threshold. Among the miRNAs that exceeded the threshold, we noted that a modest population-wide upregulation of miRNAs occurs in migratory

cINs at E15.5 compared with the progenitor populations at E13.5. A pairwise comparison between EGFP-positive and -negative populations within the MGE on E13.5 revealed 10 miRNAs that were enriched in the proliferating MGE-derived cells, 6 of which were further enriched in the migratory MGE-cINs in E15.5 cortex (Supplementary Fig. 3, Supplementary Table 4).

When we compared the relative miRNA expression in cortical MGE interneurons at E15.5 with *Nkx2.1*^{Cre} derived progenitors at E13.5, we identified 27 mature miRNAs that were significantly enriched in postmitotic MGE-derived cINs at E15.5 compared with E13.5 progenitors ($FC \geq 2$, $P < 0.01$) (Supplementary Table 3). None of the miRNAs were upregulated in the progenitor populations at E13.5 compared with MGE-derived cINs at E15.5. We confirmed the expression levels of selected miRNAs by qRT-PCR performed on independently collected EGFP-expressing cells from cortex at E15.5 and MGE at E13.5 (Fig. 8*B*). Our results showed that several members of the let7 family, miR-128, miR-9, miR-125b-5p, and miR-124, which are previously implicated in differentiation of several cell types in the CNS, were upregulated in postmitotic MGE-cINS compared with MGE progenitors (Volvert et al. 2012). MGE-cINs at E15.5 also showed increased expression of miR-15a, miR-30a, and miR106b, miRNAs that have not yet been investigated in the context of neural differentiation or survival (Bonci et al. 2008; Ivanovska et al. 2008; Ouzounova et al. 2013), as well as miR181, which has recently shown to be highly enriched in GABAergic medium spiny neurons in the nucleus accumbens (Saba et al. 2012). Nonetheless, our array analysis did not detect a large difference in miRNA expression between different cell types within the cortex (E15.5 EGFP$^+$ vs. E15.5 EGFP$^-$, $P > 0.01$) (Supplementary Fig. 3, Supplementary Table 5). Therefore, temporally upregulated miRNAs may act on common genes in different cell types or, alternatively, it is possible that the same miRNAs in EGFP$^+$ and EGFP$^-$ cells target cell type-specific mRNA transcripts providing a context-dependent post-transcriptional regulation of gene expression.

To evaluate if the mRNAs that were upregulated in the absence of *Dicer* (Fig. 7) were bona fide physiological targets of miRNAs differentially expressed in postmitotic MGE-derived cINs (Fig. 8*B*), we performed an in silico target prediction using web-based prediction algorithms.(Grimson et al. 2007; Maragkakis et al. 2009; Betel et al. 2010). We used the mRNAs that were differentially upregulated in the absence of *Dicer* as input and searched for miRNAs that are enriched in E15.5 MGE-cINs in TargetScan 5.2 (http://www.targetscan.org/), miRanda (http://microrna.org/), and Diana MicroT (http://diana.cslab.ece.ntua.gr/microT/). We found that *Igf1* has conserved motifs in its 3′UTR complementary to sequences of miR-let7 family and miR-9, which was predicted by all 3 of the algorithms. In addition, *Gad2* (miR106b), *Vat1* (miR-30, miR15, miR9), and *SubsP* (miR181) also contained target sites for the respective miRNAs, as predicted by at least 2 algorithms. Although, experimental validation is still needed, miRNA–mRNA target motifs in these genes could possibly reflect their requirement of post-transcriptional control by miRNAs enriched in postmitotic MGE-cINs. On the other hand, *SST*-3′UTR did not contain motifs that are targeted by any of the miRNAs enriched in E15.5 MGE-INs; and *NPY* was predicted to contain sites for miR-30 only by one of the algorithm (miRanda). Hence, misexpression of these mRNAs in the absence of *Dicer* is likely due to mechanisms secondary to loss of miRNAs in MGE-derived cINs. Nonetheless, more experiments are required to explore the causal role of miRNA-mediated regulation of genes such as *Igf1* in the phenotypes we observed in *Dicer* mutant MGE-cINs.

Discussion

miRNAs are necessary for the development of many distinct cell types in the nervous system (Fineberg et al. 2009); however, their requirement in cortical interneurons has not been explored. In this work, we specifically removed *Dicer* from MGE-derived cINs, therefore abolishing the production of mature miRNAs. Our results show that the loss of miRNAs, while having no impact on proliferation and the initiation of tangential migration, appears essential for the transition from tangential to radial migration as well as the subsequent survival and maturation of cINs into their specific subtypes.

The MGE is the major source of PV- and SST-expressing cINs, which represent the majority (~70%) of all interneurons in the cortex (Wonders and Anderson 2006; Rudy et al. 2011). Development of MGE-derived cINs depends on the highly ordered genetic regulation mediated by numerous transcription factors including the *Dlx* family of genes, *Nkx2.1*, *Lhx6*, and *Sox6*, which are expressed throughout the ventral telencephalon and control the specification, migration, and differentiation of MGE-cIN subtypes (Wonders and Anderson 2006; Batista-Brito and Fishell 2009). Here, we found that post-transcriptional modulation by miRNAs is essential for the proper maturation of PV- and SST-expressing cINs. However, even though there was a significant reduction in the number of cINs in the cortex by P21, miRNA depletion did not alter the number of cIN progenitors generated from the MGE (Fig. 4), their ability to initiate tangential migration toward the dorsal telencephalon (Fig. 4), or their GABAergic identity (Fig. 3). Nonetheless, almost half of the fate-mapped mutant neurons have lost their mature subtype marker expression (PV or SST) and exhibited defects in their morphology. The absence of PV or SST in a subset of mutant cells does not appear to be due to transfating of mutant cINs, as we did not detect a concomitant increase in the number of cells expressing markers characteristic of CGE-derived cINs, as seen in conditional *Nkx2.1* mutant MGE-derived cINs (Butt et al. 2008). Furthermore, the expression of GABAergic lineage genes such as *Dlx1/2*, or MGE lineage genes such as *Nkx2.1*, *Lhx6*, or Sox6 were not altered in the subpallium of E13.5 Dicer mutant animals (data not shown), or in mutant MGE-derived cINs that have migrated to the cortex at E15.5 (Supplementary Table 2).

Precocious Gene Expression of Dicer-Deficient MGE-Derived cINs Within the IZ/SVZ

Our study is consistent with growing evidence that miRNA-mediated pathways are an essential component of neuronal differentiation programs (Wu and Belasco 2005; Conaco et al. 2006; Krichevsky et al. 2006; Makeyev et al. 2007; Choi et al. 2008). In the absence of *Dicer*, MGE-derived cINs within the P21 cortex fail to express molecular markers characteristic of their subtype identity (Fig. 3). Curiously, we observed the precocious expression of *Sst*, *NPY*, and *Gad65* in cINs of E15.5 Dicer mutant animals (Fig. 7). This suggests that miRNAs regulate the onset of expression of genes specific to cINs, and in their absence, cINs initiate expression of such genes

precociously, paradoxically resulting in a reduction of IN-specific genes at later ages (Fig. 3). In P21 Dicer mutant animals, we observed a larger decrease in the number of cINs expressing PV relatively to the ones expressing SST, indicating that specification defects are much stronger in PV-expressing than in SST-expressing cIN (Fig. 3). One possibility is that miRNAs block the initiation of the genetic program in cINs destined to be PV-INs. This raises the possibility that, in the absence of miRNAs, the misexpression of *Sst* occurs within PV-IN precursors. If so, *Sst* misexpression could conflict with other molecular cues expressed by PV-IN precursors, resulting in defects in their specification and survival. In addition, precocious specification of cIN precursors might abnormally trigger the apoptotic machinery, a hypothesis that is consistent with the increased number of cells undergoing apoptosis in mutant animals specifically in the IZ/SVZ migratory zone where we also detected increased *Sst*, *NPY*, and *Gad65* expression (Figs. 6 and 7).

Previous studies that have examined the specification of PV and SST cINs have shown that, in the absence of the transcription factors, *Lhx6*, *Sox6*, and *Satb1* in MGE-derived cINs had decreased expression of PV and SST in these cell types (Liodis et al. 2007; Zhao et al. 2008; Azim et al. 2009; Batista-Brito et al. 2009; Close et al. 2012; Denaxa et al. 2012). Conversely, Denaxa et al. (2012) found that in vitro transfection of *Satb1* into dissociated MGE cells lead to an increased expression of Sst and NPY proteins, inducing a mature molecular phenotype in MGE precursors. Yet, in *Dicer* mutant, MGE-cINs increased expression of cIN subtype genes *Sst*, *NPY*, and *Gad65* is not concomitant with changes in *Lhx6*, *Sox6*, and *Satb1* expression (data not shown, Supplementary Table2). We therefore suggest that miRNA-dependent mechanisms do not act through previously identified genetic cascades that regulate MGE-derived cIN differentiation/maturation.

MGE-Derived cIN-Specific miRNA-Mediated Programs

Understanding how the miRNAs exert their effect of MGE-cIN development ultimately will require elucidating the effects resulting from removal of the precise miRNAs expressed in developing cINs and the mRNA targets that they regulate. To test whether there is a causal link between miRNA-dependent mechanisms and the cellular phenotypes observed in *Dicer* mutant MGE-cINs, we first determined that the absence of *Dicer* in these cells leads to altered gene regulation (Supplementary Table 2). Comparison of the gene expression profile of *Dicer* mutant and control MGE-derived cINs revealed abnormal upregulation of genes that are known to be important for differentiation in other cell types (such as *Npnt*, *Pou3f4*, *Dlk1*) as well as genes encoding transcription factors (such as *Magel2*, *Klf6*, *Ebf1*), which may broadly alter genetic programs involved in neuronal differentiation. We also found that genes identified with mature interneuron subtype markers (such as *Sst*, *Gad65*, *Npy*) are upregulated, which could be associated with the maturation defects we observed in P21 MGE-derived cINs (Fig. 2 and 3). Genes that mediate cellular interactions (such as *Mbc2*, *Pcdh21*, *Cdh22*) were also upregulated, which may be responsible for the radial migration defects (Fig. 5). On the other hand, upregulation of survival factors *Igf1*, *Rreb1*, *Pde1a* could be directly associated with increased MGE-cIN death within the migratory IZ/SVZ zone of mutant embryos (Fig. 6). Nevertheless, we acknowledge that a causal relationship between abnormal expression of these genes and the cellular phenotypes we observed in *Dicer* conditional mutant MGE-cINs remains elusive. It remains possible that instead of reflecting a direct regulation by miRNAs, their abnormal expression could result from a global dsyregulation of MGE-cINs.

To identify the pool of miRNAs that could potentially mediate the observed phenotypes, we compared the miRNA content of MGE-derived postmitotic cINs within the cortex with the content of miRNAs in MGE progenitors (where removal of miRNAs does not show a phenotype). In agreement with previous studies showing that the expression levels of miRNAs change dynamically during development (Krichevsky et al. 2003; Miska et al. 2004; Sempere et al. 2004), we also found that miRNA expression in cINs is temporally upregulated in postmitotic neurons compared with to the progenitors that gave rise to them (Fig. 8, Supplementary Table 3). However, our miRNA array analysis did not reveal large differences in the miRNAs expressed in $EGFP^+$ MGE-cINs compared with $EGFP^-$ non-MGE populations. We found significant temporal enrichment in miRNAs such as *let7-b*, *miR128*, *miR125b-5p*, *miR9* and *miR124* in E15.5 MGE-cINs compared with E13.5 MGE progenitors, but these miRNAs have high expression levels in the pyramidal neurons in the cortex as well (Supplementary Table 5) (Volvert et al. 2012). Such a large overlap between miRNA expression between $EGFP^+$ and $EGFP^-$ populations might suggest a scenario whereby temporally upregulated miRNAs act on common pathways in different cell types. However, it is also possible that same miRNA repertoire in $EGFP^+$ and $EGFP^-$ cells target cell type-specific mRNA transcripts provide a context-dependent post-transcriptional regulation of gene expression. Our gene expression analysis in *Dicer* mutant MGE-cINs (Fig. 7, Supplementary Table 2) did not however detect abnormal expression of genes implicated in neuronal differentiation such as *Tlx*, *Foxg1*, *Ptbp1*, which were previously reported to be targeted by broadly expressed miRNAs, such as *let7-b*, *miR-9*, and *miR-124*, respectively (Volvert et al. 2012). Instead, we showed that expression of *Igf1*, a broadly expressed survival factor, was significantly altered in *Dicer* mutant MGE-cINs, which contains conserved target sites for *let7* and *miR-9*, 2 of the highly enriched miRNAs in E15.5 MGE-cINs. In addition, we observed altered expression of *Gad2*, the GABA synthesizing enzyme specific to interneurons, in *Dicer* mutant MGE-cINs, which contains complementary target sites for miR106b. Nevertheless, these 2 examples at present only provide correlative evidence for a role for miRNA-mediated post-trancriptional control in interneurons. Further experiments are required to determine whether broadly expressed miRNAs act on common pathways involved in differentiation and/or survival or miRNA–mRNA interaction is cell type and context dependent.

Our miRNA microarray analysis did not reveal any miRNA that was significantly enriched in progenitors compared with postmitotic cINs. Instead, we observed a dynamic upregulation in the miRNA content as the MGE-cINs exit proliferative zones and become migratory. Our miRNA profiling results are in line with our observation that postmitotic removal of *Dicer* activity (mediated by the $Lhx6^{cre}$ driver) resulted in a similar, albeit milder, phenotype than *Dicer* ablation within progenitor zones using the $Nkx2.1^{cre}$ driver. Nonetheless, we cannot rule out the presence of rare miRNAs that are expressed in low levels in MGE progenitors that are beyond our detection limits. Indeed, we observed that 13 of the control probes and 39 of the mouse viral miRNAs in the microarray did not show differences in expression between 4 different cell types analyzed on the microarrays. Hence, we remain concerned that our miRNA

microarrays did not provide sufficient sensitivity to detect differences in low-expressing cell type-specific miRNAs. Perhaps, application of the recently described approach of miRNA tagging and affinity-purification (miRAP) method in combination with miRNA profiling with deep sequencing (He et al. 2012) would in our context prove more sensitive. Alternatively, it is also possible that the expression of specific miRNAs increases during maturation of cIN subtypes. Hence, it will be important to determine whether differences exist in miRNA repertories expressed in developing versus adult PV- and SST-expressing cINs.

Taken together, our work unveils the necessity of miRNAs for different aspects of inhibitory neuron development and suggests putative molecular elements that are likely to mediate particular developmental events.

Supplementary Material

Supplementary can be found at: http://www.cercor.oxfordjournals.org/.

Funding

This work is supported by NIH grants RO1MH071679, RO1MH095147, R01NS081297, and P0NS074972, the Simons Foundation, and New York State through the NYSTEM initiative to G.F.

Notes

We thank the members of the Fishell laboratory for helpful comments on this work, Lihong Yin for excellent technical help on genotyping animals, and Dr Polyxeni Philippidou for kind assistance on RT-PCR experiments. We thank Drs Chin Xu and Stewart Anderson for the *Nkx2.1BAC*^{Cre} driver, Dr Cliff Tabin for the Dicer conditional line, Dr Nicoletta Kessaris for *Lhx6BAC*^{Cre} driver, and Dr Sonia Garel for the Ebf1 cDNA. *Conflict of Interest*: None declared.

References

Ang ES Jr, Haydar TF, Gluncic V, Rakic P. 2003. Four-dimensional migratory coordinates of GABAergic interneurons in the developing mouse cortex. J Neurosci. 23:5805–5815.

Ashburner M, Ball CA, Blake JA, Botstein D, Butler H, Cherry JM, Davis AP, Dolinski K, Dwight SS, Eppig JT et al. 2000. Gene ontology: tool for the unification of biology. The Gene Ontology Consortium. Nat Genet. 25:25–29.

Azim E, Jabaudon D, Fame RM, Macklis JD. 2009. SOX6 controls dorsal progenitor identity and interneuron diversity during neocortical development. Nat Neurosci. 12:1238–1247.

Bartel DP. 2009. MicroRNAs: target recognition and regulatory functions. Cell. 136:215–233.

Batista-Brito R, Fishell G. 2009. The developmental integration of cortical interneurons into a functional network. Curr Top Dev Biol. 87:81–118.

Batista-Brito R, Machold R, Klein C, Fishell G. 2008. Gene expression in cortical interneuron precursors is prescient of their mature function. Cereb Cortex. 18:2306–2317.

Batista-Brito R, Rossignol E, Hjerling-Leffler J, Denaxa M, Wegner M, Lefebvre V, Pachnis V, Fishell G. 2009. The cell-intrinsic requirement of Sox6 for cortical interneuron development. Neuron. 63:466–481.

Betel D, Koppal A, Agius P, Sander C, Leslie C. 2010. Comprehensive modeling of microRNA targets predicts functional non-conserved and non-canonical sites. Genome Biol. 11:R90.

Bonci D, Coppola V, Musumeci M, Addario A, Giuffrida R, Memeo L, D'Urso L, Pagliuca A, Biffoni M, Labbaye C et al. 2008. The miR-15a-miR-16-1 cluster controls prostate cancer by targeting multiple oncogenic activities. Nat Med. 14:1271–1277.

Butt SJ, Sousa VH, Fuccillo MV, Hjerling-Leffler J, Miyoshi G, Kimura S, Fishell G. 2008. The requirement of Nkx2-1 in the temporal specification of cortical interneuron subtypes.[see comment]. Neuron. 59:722–732.

Cammenga J, Mulloy JC, Berguido FJ, MacGrogan D, Viale A, Nimer SD. 2003. Induction of C/EBPalpha activity alters gene expression and differentiation of human CD34+ cells. Blood. 101:2206–2214.

Cheloufi S, Dos Santos CO, Chong MM, Hannon GJ. 2010. A dicer-independent miRNA biogenesis pathway that requires Ago catalysis. Nature. 465:584–589.

Choi PS, Zakhary L, Choi WY, Caron S, Alvarez-Saavedra E, Miska EA, McManus M, Harfe B, Giraldez AJ, Horvitz HR et al. 2008. Members of the miRNA-200 family regulate olfactory neurogenesis. Neuron. 57:41–55.

Close J, Xu H, De Marco Garcia N, Batista-Brito R, Rossignol E, Rudy B, Fishell G. 2012. Satb1 is an activity-modulated transcription factor required for the terminal differentiation and connectivity of medial ganglionic eminence-derived cortical interneurons. J Neurosci. 32:17690–17705.

Conaco C, Otto S, Han JJ, Mandel G. 2006. Reciprocal actions of REST and a microRNA promote neuronal identity. Proc Natl Acad Sci USA. 103:2422–2427.

Davis TH, Cuellar TL, Koch SM, Barker AJ, Harfe BD, McManus MT, Ullian EM. 2008. Conditional loss of Dicer disrupts cellular and tissue morphogenesis in the cortex and hippocampus. J Neurosci. 28:4322–4330.

de Chevigny A, Core N, Follert P, Gaudin M, Barbry P, Beclin C, Cremer H. 2012. miR-7a regulation of Pax6 controls spatial origin of forebrain dopaminergic neurons. Nat Neurosci. 15:1120–1126.

Denaxa M, Kalaitzidou M, Garefalaki A, Achimastou A, Lasrado R, Maes T, Pachnis V. 2012. Maturation-promoting activity of SATB1 in MGE-derived cortical interneurons. Cell Rep. 2:1351–1362.

De Pietri Tonelli D, Pulvers JN, Haffner C, Murchison EP, Hannon GJ, Huttner WB. 2008. miRNAs are essential for survival and differentiation of newborn neurons but not for expansion of neural progenitors during early neurogenesis in the mouse embryonic neocortex. Development. 135:3911–3921.

Dugas JC, Cuellar TL, Scholze A, Ason B, Ibrahim A, Emery B, Zamanian JL, Foo LC, McManus MT, Barres BA. 2010. Dicer1 and miR-219 are required for normal oligodendrocyte differentiation and myelination. Neuron. 65:597–611.

Farh KK, Grimson A, Jan C, Lewis BP, Johnston WK, Lim LP, Burge CB, Bartel DP. 2005. The widespread impact of mammalian microRNAs on mRNA repression and evolution. Science. 310:1817–1821.

Filipowicz W, Bhattacharyya SN, Sonenberg N. 2008. Mechanisms of post-transcriptional regulation by microRNAs: are the answers in sight? Nat Rev Genet. 9:102–114.

Fineberg SK, Kosik KS, Davidson BL. 2009. MicroRNAs potentiate neural development. Neuron. 64:303–309.

Fogarty M, Grist M, Gelman D, Marin O, Pachnis V, Kessaris N. 2007. Spatial genetic patterning of the embryonic neuroepithelium generates GABAergic interneuron diversity in the adult cortex. J Neurosci. 27:10935–10946.

Gao FB. 2008. Posttranscriptional control of neuronal development by microRNA networks. Trends Neurosci. 31:20–26.

Garcia-Dominguez M, Poquet C, Garel S, Charnay P. 2003. Ebf gene function is required for coupling neuronal differentiation and cell cycle exit. Development. 130:6013–6025.

Garel S, Marin F, Grosschedl R, Charnay P. 1999. Ebf1 controls early cell differentiation in the embryonic striatum. Development. 126:5285–5294.

Grimson A, Farh KK, Johnston WK, Garrett-Engele P, Lim LP, Bartel DP. 2007. MicroRNA targeting specificity in mammals: determinants beyond seed pairing. Mol Cell. 27:91–105.

Hanashima C, Li SC, Shen L, Lai E, Fishell G. 2004. Foxg1 suppresses early cortical cell fate. Science. 303:56–59.

Harfe BD, McManus MT, Mansfield JH, Hornstein E, Tabin CJ. 2005. The RNaseIII enzyme Dicer is required for morphogenesis but not patterning of the vertebrate limb. Proc Natl Acad Sci USA. 102:10898–10903.

He M, Liu Y, Wang X, Zhang MQ, Hannon GJ, Huang ZJ. 2012. Cell-type-based analysis of microRNA profiles in the mouse brain. Neuron. 73:35–48.

Hevner RF, Shi L, Justice N, Hsueh Y, Sheng M, Smiga S, Bulfone A, Goffinet AM, Campagnoni AT, Rubenstein JL. 2001. Tbr1 regulates differentiation of the preplate and layer 6. Neuron. 29:353–366.
Inan M, Welagen J, Anderson SA. 2012. Spatial and temporal bias in the mitotic origins of somatostatin- and parvalbumin-expressing interneuron subgroups and the chandelier subtype in the medial ganglionic eminence. Cereb Cortex. 22:820–827.
Ivanovska I, Ball AS, Diaz RL, Magnus JF, Kibukawa M, Schelter JM, Kobayashi SV, Lim L, Burchard J, Jackson AL et al. 2008. MicroRNAs in the miR-106b family regulate p21/CDKN1A and promote cell cycle progression. Mol Cell Biol. 28:2167–2174.
Karres JS, Hilgers V, Carrera I, Treisman J, Cohen SM. 2007. The conserved microRNA miR-8 tunes atrophin levels to prevent neurodegeneration in Drosophila. Cell. 131:136–145.
Kim J, Inoue K, Ishii J, Vanti WB, Voronov SV, Murchison E, Hannon G, Abeliovich A. 2007. A microRNA feedback circuit in midbrain dopamine neurons. Science. 317:1220–1224.
Krek A, Grun D, Poy MN, Wolf R, Rosenberg L, Epstein EJ, MacMenamin P, da Piedade I, Gunsalus KC, Stoffel M et al. 2005. Combinatorial microRNA target predictions. Nat Genet. 37:495–500.
Krichevsky AM, King KS, Donahue CP, Khrapko K, Kosik KS. 2003. A microRNA array reveals extensive regulation of microRNAs during brain development. RNA. 9:1274–1281.
Krichevsky AM, Sonntag KC, Isacson O, Kosik KS. 2006. Specific microRNAs modulate embryonic stem cell-derived neurogenesis. Stem Cells. 24:857–864.
Lavdas AA, Grigoriou M, Pachnis V, Parnavelas JG. 1999. The medial ganglionic eminence gives rise to a population of early neurons in the developing cerebral cortex. J Neurosci. 19:7881–7888.
Lee S, Hjerling-Leffler J, Zagha E, Fishell G, Rudy B. 2010. The largest group of superficial neocortical GABAergic interneurons expresses ionotropic serotonin receptors. J Neurosci. 30:16796–16808.
Levitt P, Eagleson KL, Powell EM. 2004. Regulation of neocortical interneuron development and the implications for neurodevelopmental disorders. Trends Neurosci. 27:400–406.
Lewis BP, Shih IH, Jones-Rhoades MW, Bartel DP, Burge CB. 2003. Prediction of mammalian microRNA targets. Cell. 115:787–798.
Lewis DA, Hashimoto T, Volk DW. 2005. Cortical inhibitory neurons and schizophrenia. Nat Rev Neurosci. 6:312–324.
Lim LP, Lau NC, Garrett-Engele P, Grimson A, Schelter JM, Castle J, Bartel DP, Linsley PS, Johnson JM. 2005. Microarray analysis shows that some microRNAs downregulate large numbers of target mRNAs. Nature. 433:769–773.
Liodis P, Denaxa M, Grigoriou M, Akufo-Addo C, Yanagawa Y, Pachnis V. 2007. Lhx6 activity is required for the normal migration and specification of cortical interneuron subtypes. J Neurosci. 27:3078–3089.
Livak KJ, Schmittgen TD. 2001. Analysis of relative gene expression data using real-time quantitative PCR and the 2(-Delta Delta C(T)) Method. Methods. 25:402–408.
Llorens-Martin M, Torres-Aleman I, Trejo JL. 2009. Mechanisms mediating brain plasticity: IGF1 and adult hippocampal neurogenesis. Neuroscientist. 15:134–148.
Makeyev EV, Zhang J, Carrasco MA, Maniatis T. 2007. The microRNA miR-124 promotes neuronal differentiation by triggering brain-specific alternative pre-mRNA splicing. Mol Cell. 27:435–448.
Maragkakis M, Reczko M, Simossis VA, Alexiou P, Papadopoulos GL, Dalamagas T, Giannopoulos G, Goumas G, Koukis E, Kourtis K et al. 2009. DIANA-microT web server: elucidating microRNA functions through target prediction. Nucleic Acids Res. 37:W273–W276.
Marin O, Rubenstein JL. 2001. A long, remarkable journey: tangential migration in the telencephalon. Nat Rev Neurosci. 2:780–790.
Markram H, Toledo-Rodriguez M, Wang Y, Gupta A, Silberberg G, Wu C. 2004. Interneurons of the neocortical inhibitory system. Nat Rev Neurosci. 5:793–807.
Miska EA, Alvarez-Saavedra E, Townsend M, Yoshii A, Sestan N, Rakic P, Constantine-Paton M, Horvitz HR. 2004. Microarray analysis of microRNA expression in the developing mammalian brain. Genome Biol. 5:R68.
Miyoshi G, Butt SJ, Takebayashi H, Fishell G. 2007. Physiologically distinct temporal cohorts of cortical interneurons arise from telencephalic Olig2-expressing precursors. J Neurosci. 27:7786–7798.
Miyoshi G, Fishell G. 2011. GABAergic interneuron lineages selectively sort into specific cortical layers during early postnatal development. Cereb Cortex. 21:845–852.
Moore CI, Carlen M, Knoblich U, Cardin JA. 2010. Neocortical interneurons: from diversity, strength. Cell. 142:189–193.
Nery S, Fishell G, Corbin JG. 2002. The caudal ganglionic eminence is a source of distinct cortical and subcortical cell populations. Nat Neurosci. 5:1279–1287.
Ouzounova M, Vuong T, Ancey PB, Ferrand M, Durand G, Le-Calvez Kelm F, Croce C, Matar C, Herceg Z, Hernandez-Vargas H. 2013. MicroRNA miR-30 family regulates non-attachment growth of breast cancer cells. BMC Genomics. 14:139.
Ozdinler PH, Macklis JD. 2006. IGF-I specifically enhances axon outgrowth of corticospinal motor neurons. Nat Neurosci. 9:1371–1381.
Petilla Interneuron Nomenclature G, Ascoli GA, Alonso-Nanclares L, Anderson SA, Barrionuevo G, Benavides-Piccione R, Burkhalter A, Buzsaki G, Cauli B, Defelipe J et al. 2008. Petilla terminology: nomenclature of features of GABAergic interneurons of the cerebral cortex. Nat Rev Neurosci. 9:557–568.
Polleux F, Whitford KL, Dijkhuizen PA, Vitalis T, Ghosh A. 2002. Control of cortical interneuron migration by neurotrophins and PI3-kinase signaling. Development. 129:3147–3160.
Rajasekhar VK, Viale A, Socci ND, Wiedmann M, Hu X, Holland EC. 2003. Oncogenic Ras and Akt signaling contribute to glioblastoma formation by differential recruitment of existing mRNAs to polysomes. Mol Cell. 12:889–901.
Rudy B, Fishell G, Lee S, Hjerling-Leffler J. 2011. Three groups of interneurons account for nearly 100% of neocortical GABAergic neurons. Dev Neurobiol. 71:45–61.
Saba R, Storchel PH, Aksoy-Aksel A, Kepura F, Lippi G, Plant TD, Schratt GM. 2012. Dopamine-regulated microRNA MiR-181a controls GluA2 surface expression in hippocampal neurons. Mol Cell Biol. 32:619–632.
Schaefer A, O'Carroll D, Tan CL, Hillman D, Sugimori M, Llinas R, Greengard P. 2007. Cerebellar neurodegeneration in the absence of microRNAs. J Exp Med. 204:1553–1558.
Sempere LF, Freemantle S, Pitha-Rowe I, Moss E, Dmitrovsky E, Ambros V. 2004. Expression profiling of mammalian microRNAs uncovers a subset of brain-expressed microRNAs with possible roles in murine and human neuronal differentiation. Genome Biol. 5:R13.
Shibata M, Kurokawa D, Nakao H, Ohmura T, Aizawa S. 2008. MicroRNA-9 modulates Cajal-Retzius cell differentiation by suppressing Foxg1 expression in mouse medial pallium. J Neurosci. 28:10415–10421.
Sousa VH, Miyoshi G, Hjerling-Leffler J, Karayannis T, Fishell G. 2009. Characterization of Nkx6-2-derived neocortical interneuron lineages. Cereb Cortex. 19(Suppl 1):i1–10.
Taniguchi H, Lu J, Huang ZJ. 2013. The spatial and temporal origin of chandelier cells in mouse neocortex. Science. 339:70–74.
Volvert ML, Rogister F, Moonen G, Malgrange B, Nguyen L. 2012. MicroRNAs tune cerebral cortical neurogenesis. Cell Death Differ. 19:1573–1581.
Whittington MA, Traub RD. 2003. Interneuron diversity series: inhibitory interneurons and network oscillations in vitro. Trends Neurosci. 26:676–682.
Wonders CP, Anderson SA. 2006. The origin and specification of cortical interneurons. Nat Rev Neurosci. 7:687–696.
Wu L, Belasco JG. 2005. Micro-RNA regulation of the mammalian lin-28 gene during neuronal differentiation of embryonal carcinoma cells. Mol Cell Biol. 25:9198–9208.
Xu Q, Tam M, Anderson SA. 2008. Fate mapping Nkx2.1-lineage cells in the mouse telencephalon. J Comp Neurol. 506:16–29.
Ye P, D'Ercole AJ. 2006. Insulin-like growth factor actions during development of neural stem cells and progenitors in the central nervous system. J Neurosci Res. 83:1–6.
Zhao Y, Flandin P, Long JE, Cuesta MD, Westphal H, Rubenstein JL. 2008. Distinct molecular pathways for development of telencephalic interneuron subtypes revealed through analysis of Lhx6 mutants. J Comp Neurol. 510:79–99.